GUARDRAIL IMPACT SIMULATION
FOR REMOTE GUIDED VEHICLES (RGV'S)
USED IN NUCLEAR GENERATING STATIONS

Ahmed Abbas

BEng, Concordia University, 2012

A MRP

presented to Ryerson University

in partial fulfillment of the

requirements for the degree of

Master of Engineering

in the program of

Civil Engineering

Toronto, Ontario, Canada, 2018

AUTHOR'S DECLARATION
FOR ELECTRONIC SUBMISSION OF A MRP

I hereby declare that I am the sole author of this MRP. This is a true copy of the MRP, including any required final revisions.

I authorize Ryerson University to lend this MRP to other institutions or individuals for the purpose of scholarly research.

I further authorize Ryerson University to reproduce this MRP by photocopying or by other means, in total or in part, at the request of other institutions or individuals for the purpose of scholarly research.

I understand that my MRP may be made electronically available to the public.

GUARDRAIL IMPACT SIMULATION FOR REMOTE GUIDED VEHICLES (RGV'S) USED IN NUCLEAR GENERATING STATIONS

Ahmed Abbas

Master of Engineering in Civil

Engineering Ryerson University, 2018

ABSTRACT

During nuclear station refurbishment, transportation of tools, equipment, and irradiated reactor components is achieved using remote guided vehicles (RGV's) in order to keep worker radiation doses as low as reasonably achievable.

A removable guardrail system capable of withstanding RGV impact was developed to eliminate the risk of accidents taking place in the reactor vault. The guardrails are mounted to platform edges using two bolts and two shear pins. In anticipation of frequent removal of reinstallation of guardrails by workers, this study proposes that guardrails be installed without bolting, relying solely on the guardrails' shear pins to provide the required restraint.

A parametric impact simulation was carried out in order to evaluate the performance of the guardrails when installed without bolting. The analysis work was carried out using LS-DYNA, an advanced simulation software package capable of simulating real world problems using explicit time integration.

ACKNOWLEDGEMENTS

DEDICATION

This work is dedicated to my father.

TABLE OF CONTENTS

LIST OF TABLES

LIST OF FIGURES

1 INTRODUCTION

1.1 Purpose and Background

As major components of a nuclear generating station approach their end of life, the station undergoes a major refurbishment effort to extend the facility's life and maintain its license to operate. While the refurbishment effort typically consists of a number of distinct activities that vary in scale, the largest and most significant activity is the retubing and feeder replacement (RFR), where the pressure tubes, calandria tubes, and feeders in each reactor are removed and replaced. [R.1][R.2]

The RFR activity involves manipulating tools and equipment and transporting spent and irradiated reactor components across a variety of platforms erected inside the reactor vault. In order to keep worker radiation doses as low as reasonably achievable, handling and transportation is achieved remotely using remote guided vehicles (RGV's). [R.1]

While administrative controls and procedures are employed to ensure that operation of remote handling equipment is carried out safely, a modular guardrail system was developed for use in the reactor vault as a second line of defense to eliminate the risk of serious accidents taking place in case of stalling or operator error while RGV's travel across the different platforms. As designed, the guardrail modules are mounted using two bolts and two shear pins.

During the refurbishment effort, it is anticipated that removal and reinstallation of guardrails by workers will be frequently required in order to allow RGV's to travel from one platform to another. To address the challenge of creating a guardrail system that is easily removable yet capable of withstanding large impact forces, this study proposes that guardrail modules be installed without bolting, relying solely on the guardrails' shear pins to provide the required restraint. This would facilitate removal and reinstallation of guardrail modules and minimize workers' exposure to radiation.

1.2 Guardrail and RGV Description

1.2.1 Platform and Guardrail System

As described above, a number of platforms will be erected inside the reactor vault during the refurbishment effort. The platform of interest in this study is built up of stacked modules fabricated from structural steel, with the top module supporting a working surface upon which the RGV's will travel (see Figure 1). The top module's outer beams, which are laterally braced by cross-beams at 32-inch centers, provide an interface for mounting the guardrail system (see Figure 2).

Figure 1.   **The platform considered in this study consists of stacked modules.**

The guardrail system consists of modules built up of structural steel plates that provide a curb (4-1/2 inches in height) designed to withstand the impact of a fully-loaded RGV. The modules, shown in Figure 3, are each 32 inches in length and use two bolts and two shear pins to mount onto the platform's outer beams.

Figure 2. **The mounting interface accommodates two bolts and two pins.**

(a)

(b)

Figure 3. **(a) guardrail module (b) shear pins attached to module's underside.**

1.2.2   Remote Guided Vehicle (RGV's)

This study is based on the 50-ton capacity RGV manufactured by Wheelift and slated for use during the refurbishment effort. It consists of a load-carrying frame equipped with motion sensors and an electric, self-propelled drive system. The motion sensors failsafe the RGV by disabling the vehicle when impact is detected. A lateral impact load of 45,000 pounds is prescribed by the manufacturer for a fully-loaded RGV travelling at the maximum drive speed. Figure 4 shows a 50-ton capacity RGV like the one considered in this study, and Figure 5 shows an example of an RGV transporting equipment in an industrial plant. [R.3]

The RGV's load-carrying frame has overall measurements of 164 inches in length and 79 inches in width, and is outfitted with a fluid suspension capable of raising and lowering the frame. The electric drive system consists of four wheelsets. The wheelsets each consist of electric motors powering two wheels connected to an independent on-center rotating axle, providing the RGV with omni-directional travel capability (see Figure 6). At the vehicle's nominal drive height, the lowest part of the frame would be 3 to 4 inches above the working surface. Thus, it is considered in this study that upon impact, the frame, and not the wheelsets, will come in contact with the guardrail. [R.3]

Figure 4.   **50-Ton Capacity RGV [R.3]**

Figure 5.   **An RGV transporting equipment in an industrial plant. [R.3]**

Figure 6.   **Wheelsets with independent on-center rotating axles. [R.3]**

1.3 Impact Simulation

1.3.1 Methodology

In order to evaluate the performance of the guardrail system against RGV impact when installed without bolting, a set of finite element models were generated for guardrail-beam assemblies, and a parametric impact simulation was carried out using LS-DYNA, an advanced general-purpose multi-physics simulation software package capable of simulating many complex, real world problems using explicit time integration. An overview of the theoretical basis of the software is provided in Chapter 2. [R.4]

For the purpose of evaluating the guardrails' performance during impact, two forms of output are obtained from LS-DYNA and examined:

1. The von Mises stresses in the beam assemblies are examined to ensure that the von Mises yield criterion is not exceeded during impact. The yield criterion is taken as 45,000 psi per the requirements set out in the Canadian steel design code. [R.9]
2. The deformed shapes at each output states (i.e. t=0.0 to t=0.5) are examined to ensure that the guardrail modules remain mounted and do not unlatch upon impact.

If the simulation results meet the two criteria outlined above, the performance of the guardrail system with the bolts removed is deemed acceptable.

1.3.2 Parametric Analysis

A parametric analysis was carried out in this study with three parameters nominated for evaluation and eight unique impact scenarios selected for simulation. The three parameters evaluated are: (a) impact orientation; (b) location of impact along the guardrail system; and (c) cross-beam spacing used in the platform's top module.

While the first two parameters were selected in order to address the wide range of impact scenarios made possible by the RGVs' omni-directional travel capability, the third parameter was selected in an attempt to optimize the platform design by reducing the number of cross-beams required. The range of values associated with these parameters are presented in Table 1.

Table 1.   **Outline of parameters and values considered in study**

Parameters	Values
Impact orientation	90^0 (Head-on Impact)
	60^0 (Side Impact)
Impact location	Left-hand side of module
	Center
	Right-hand side of module
Cross-beam spacing	32-inch
	64-inch
	96-inch

With the parameters selected and their value ranges established, a list of all possible parameter combinations was inspected to develop the impact scenarios considered in this study. Elimination of redundant and trivial parameter combinations yielded eight impact scenarios as outlined in Table 2.

Eight unique finite element models were generated to represent each of the impact scenarios outlined Table 2. Throughout this study, these models are referred to as *FEM-1* through *FEM-8*. Detailed description of the finite element analysis work is provided in Chapter 3.

Table 2.   **Outline of impact scenarios considered in study**

Parameter / Value Model #	Impact orientation		Impact location			Cross-beam spacing		
	90°	60°	Left	Center	Right	32-inch	64-inch	96-inch
FEM-1	●			●		●		
FEM-2		●	●			●		
FEM-3		●		●		●		
FEM-4		●			●	●		
FEM-5	●			●			●	
FEM-6		●		●			●	
FEM-7	●			●				●
FEM-8		●		●				●

2 THEORY AND BACKGROUND

2.1 Background

The impact analyses at the core of this study were carried out using LS-DYNA. The software package has its core competencies in solving highly nonlinear transient dynamic problems using explicit time integration. In addition to wide usage in the automobile and manufacturing industries to simulate crash tests and metal forming processes, LS-DYNA is seeing increasing use in the nuclear industry to perform dropped load analyses and assess the impact of accidentally dropping heavy loads in areas where fuel and reactor safety could be compromised. [R.4]

2.2 Theory

The main objective of the impact simulation carried out is calculating the displacement of the bodies under consideration through time. In LS-DYNA, this is achieved by first generating a finite element model to discretize the bodies in question and then solving for nodal displacements through time using a *time integration loop*. In this loop, the following steps (among others, see Figure 7) are performed in iteration for every time step:

1. boundary conditions are applied and elements are processed whereby relationships between nodal accelerations, velocities, and displacements are established (based on the principle of virtual work);
2. a contact-impact algorithm is applied to determine if two bodies are in contact and kinematic boundary conditions are applied accordingly;
3. nodal accelerations are calculated by numerically integrating the equations of motion (using explicit time integration);
4. velocities and nodal displacement are obtained based on the nodal accelerations calculated in step 2 and the relationships established in step 1.

While the LS-DYNA Theory Manual [R.5] provides detailed descriptions of the mathematical and physical bases of the software, the key concepts involved in the analysis work carried out are discussed below in Sections 2.2.1 through 2.2.4.
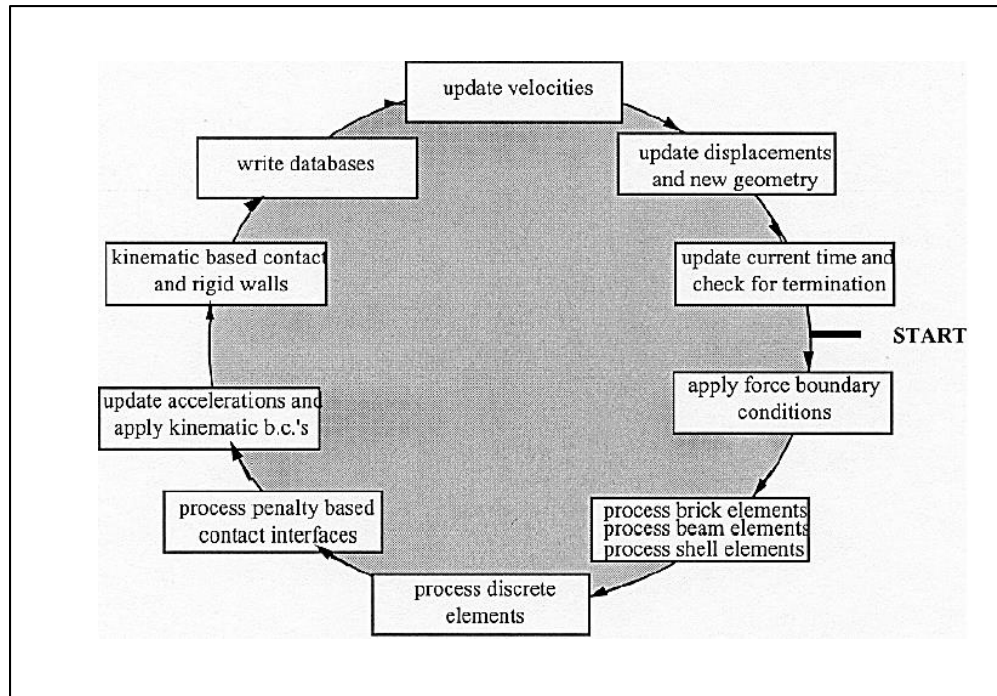

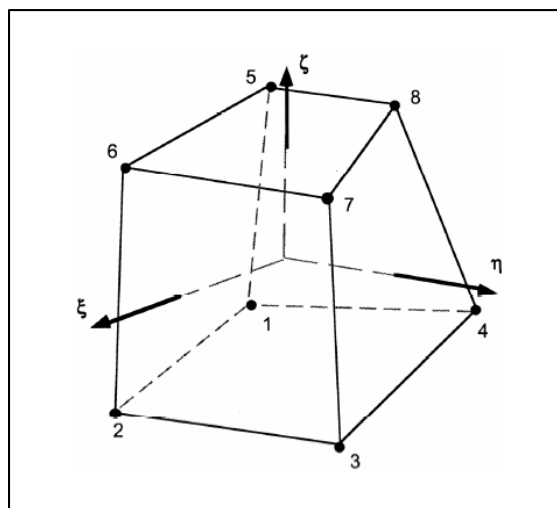Figure 7.   **The time integration loop in LS-DYNA. [R.5]**

Figure 8.   **Eight-node solid hexahedron element. [R.5]**

2.2.1 Spatial Discretization

While LS-DYNA contains a variety of element definitions, 8-node solid elements are used in this study to achieve spatial discretization and generate a polyhedral finite element mesh approximating the geometry of the beam and guardrail assemblies.

The time-dependent deformation function for a mesh of 8-note solid elements is represented by:

$$x_i\left(X_\alpha,t\right)=x_i\left(X_\alpha\left(\xi,\eta,\zeta\right),t\right)=\sum_{j=1}^{8}\phi_j\left(\xi,\eta,\zeta\right)x_i^j\left(t\right) \qquad \text{[Eq. 1]}$$

where ϕ_j are shape functions, (ξ,η,ζ) are the parametric coordinates, 8 is the number of nodes defining the elements, and x_j^i is the coordinate of the jth node in the ith direction. [R.5]

2.2.2 The Principle of Virtual Work

The principle of virtual work is used to establish a relationship between nodal accelerations and nodal displacement. The weak form of the equilibrium equation given in [Eq. 2] is applied as it provides a statement of the principle of virtual work that is suitable for numerical analysis:

$$\int_v \rho\ddot{x}_i\,\delta x_i dv+\int_v \sigma_{ij}\delta x_{i,j}dv-\int_v \rho f_i\delta x_i dv-\int_{\partial b_1} t_i\delta x_i ds = 0 \qquad \text{[Eq. 2]}$$

where ρ is the current density, $\ddot{x}$ is the acceleration, δ is the virtual displacement, x is the time-dependent deformation, σ_{ij} is the Cauchy stress, $x_{i,j}$ is the strain, f is the body force per unit volume, and t is the traction load. [R.5]

The time-dependent deformation for a mesh of solid elements given in [Eq. 1] is superimposed on the equilibrium equation given in [Eq. 2], resulting in the matrix form of the equilibrium equation:

$$\sum_{m=1}^{n}\left\{\int_{v_m}\rho N^tN a\,dv+\int_{v_m}B^t\,\sigma\,dv-\int_{v_m}\rho N^t b\,dv-\int_{\partial b_1}N^t t\,ds\right\}^m = 0 \qquad \text{[Eq. 3]}$$

11

where N is the interpolation matrix, a is the nodal acceleration vector, B is the strain-displacement matrix, σ is the stress vector, b is the body force load vector, and t is the applied traction load vector. Ultimately, LS-DYNA uses the matrix form of the equilibrium equation given in [Eq. 3] to process the nodal displacement taking place through every time step.

2.2.3 Contact-Impact Algorithm

In the impact simulations carried out in this study, an automatic surface-to-surface contact command in LS-DYNA is used, defining one body (or set of bodies) as *slave* and another body (or set of bodies) as *master* before initiating the software's contact-impact algorithm. The contact-algorithm in LS-DYNA consists of the following sequence of operations:

1. the interface between master and slave bodies is defined;
2. a "slave search" is performed to determine if a slave node and a master segment have come in contact with one another;
3. the kinematic constraint method is applied to handle sliding and impact along the interface between the slave and master bodies.

While an overview for each of these operations is provided below, these operations are discussed in greater detail in the LS-DYNA Theory Manual. [R.5]

2.2.3.1 Interface definition

The interface between the slave and the master bodies must be defined before attempting to determine if two particles have come in contact. With automatic contact commands, LS-DYNA internally generates slave and master surfaces which represent the outside facets of the discrete solid volumes being analyzed. These surfaces, which consist of a mesh of triangular and quadrilateral elements, define the interface between slave and master bodies. The triangular and quadrilateral elements that make up the slave and master surfaces are hence referred to as *master segments* and *slave segments*, respectively. Similarly, the nodes defining these segments are referred to as *slave nodes* and *master nodes*. [R.5]

2.2.3.2 Slave search

With the master and slave interface defined, a slave search is carried out to find for each slave node the nearest point on the master surface. This is achieved by first finding the nearest master node for a given slave node, then finding the master segments connected to that master node. As shown in Figure 9-a, any of these segments can harbor the slave node n_s given that m_s is the nearest master node.
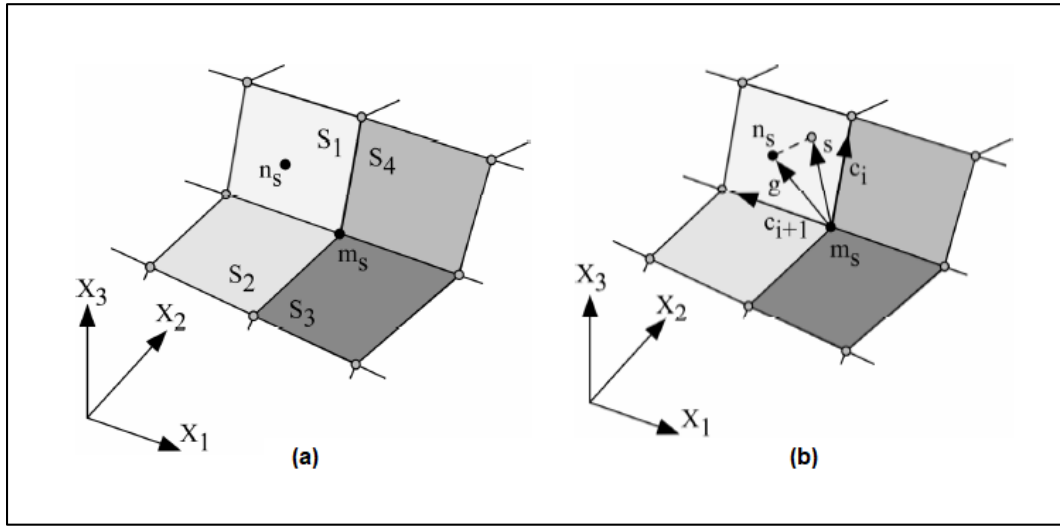

Figure 9.   **(a) segments harboring node n_s (b) vector projections on segment s_1. [R.5]**

LS-DYNA identifies the segment harboring n_s by projecting the vector g, originating at m_s and ending at n_s, onto the each of the master segments and performing a test based on the vector identified in Figure 9-b and the inequalities given in [Eq. 4]:

$$(c_i \times s) \cdot (c_i \times c_{i+1}) > 0$$

[Eq. 4]

$$(c_i \times s) \cdot (s \times c_{i+1}) > 0$$

When a contact segment is identified, the solution for the point of contact, s, becomes nontrivial. Based on this, it can be determined if and when a slave node and a master segment have come in contact with one another. [R.5]

13

2.2.3.3 Kinematic constraint method

LS-DYNA implements the kinematic constraint method to handle sliding and impact of slave nodes along the contact interface. When the slave search identifies that a slave node and a master segment have come in contact, the equations of motion for the slave and master bodies are coupled by making the displacements compatible. In addition, the impact conditions are imposed by transforming the displacement components of the slave node along the contact interface, effectively constraining the slave nodes to slide on the surface of the contact master segment and preventing penetration. [R.5][R.6]

With the slave and master bodies in contact and the slave node constrained along the contact interface, the slave node will remain on the master surface until a tensile force develops between the node and surface. [R.5]

2.2.4 Explicit Time Integration

The nodal acceleration vector is calculated by integrating the equation of motion:

$$m\ddot{u} + c\dot{u} + f_{int}(u) = p(t) \qquad \text{[Eq. 5]}$$

where m is mass, $\ddot{u}$ is acceleration, c is damping, $\dot{u}$ is velocity, $f_{int}(u)$ is internal force, and $p(u)$ is external force. [R.5]

Time integration of the equation of motion [Eq. 5] is achieved in LS-DYNA using the explicit central differencing scheme, a numerical solution methodology based on explicit time integration where the state of the system at the current time step is calculated based on the state of the system at the previous time step. While explicit solvers generally require very small time steps and thus a large number of iterations to be taken, explicit solvers are known to be convergent and numerically stable, and the smaller time steps required are considered beneficial when simulating the response of materials to severe loading over a short period. [R.5]

3   FINITE ELEMENT ANALYSIS

3.1   Model Description

Eight unique finite element models were generated for this study. In these models, guardrails and platform beam segments are modelled in configurations matching the eight impact scenarios outlined in Table 2. The models are referred to as *FEM-1* through *FEM-8*.

This section presents, the geometry, boundary conditions, materials, loads, and settings defined within each model.

3.1.1   Directional Naming Convention

The coordinate system used in all models can be seen in Figure 10. The axes are defined as follows:

- the X-axis runs along the axis of the guardrail and platform beam;
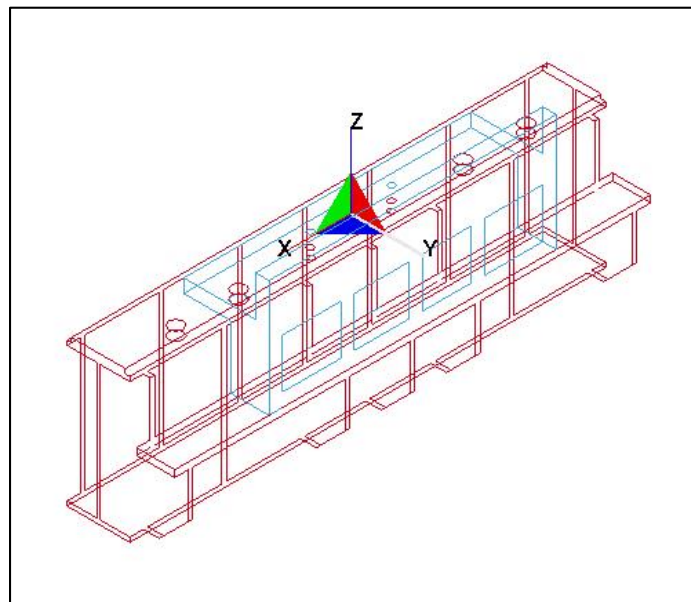- the Y-axis runs perpendicular to the guardrail; and
- the Z axis runs vertically.

Figure 10.   **FEA Coordinate System.**

3.1.2 Units

LS-DYNA requires that a consistent system of units be used, satisfying the following:

- $(1\ force\ unit) = (1\ mass\ unit) \times (1\ acceleration\ unit)$
- $(1\ acceleration\ unit) = (1\ length\ unit) \div (1\ time\ unit)^2$
- $(1\ density\ unit) = (1\ mass\ unit) \div (1\ length\ unit)^3$

The unit system used is in the analysis satisfies the conditions above and is presented in Table 3. In this system, gravity is defined as $386.4\ in/sec^2$.

Table 3.   **FEA Unit System.**

Quantities	Units
Mass	lbf-s²/in
Length	in
Time	s
Force	lbf
Stress	psi
Energy	lbf-in

3.1.3 Geometry

LS-DYNA nomenclature refers to the geometry of a finite element models as an *assembly*. Simply put, a finite element mesh representing an object in the analysis constitutes a *part*, and an arrangement of distinct *parts* constitutes an *assembly*. [R.7]

In the assemblies generated for models FEM-1 through FEM-8, each guardrail and platform beam segment is defined as a distinct part and is modelled using a mesh of eight-node solid elements with a mesh size of 1/2-inch. Descriptions are provided below for each assembly.

3.1.3.1 FEM-1 to FEM-4 Assemblies

Models FEM-1 to FEM-4 have identical assemblies consisting of one guardrail module mounted on a beam segment having a 32-inch cross-beam spacing. The assembly used in these models is shown in Figure 11.

3.1.3.2 FEM-5 Assembly

Model FEM-5 has an assembly consisting of two guardrail modules mounted on a beam segment having a 64-inch cross-beam spacing. The assembly is shown in Figure 12.

3.1.3.3 FEM-6 Assembly

Model FEM-6 has an assembly consisting of one guardrail module mounted on a beam segment having a 64-inch cross-beam spacing. The second guardrail module does not receive an impact load and is thus eliminated from the model to reduce computing time. The assembly is shown in Figure 13.

3.1.3.4 FEM-7 Assembly

Model FEM-7 has an assembly consisting of three guardrail modules mounted on a beam segment having a 96-inch cross-beam spacing. The assembly is shown Figure 14.

3.1.3.5 FEM-8 Assembly

Model FEM-8 has an assembly consisting of one guardrail modules mounted on a beam segment having a 96-inch cross-beam spacing. As only the center guardrail module receives a load in this impact scenario, the left-hand side and right-hand side guardrail modules are eliminated from the model to reduce computing time. The assembly is shown in Figure 15.
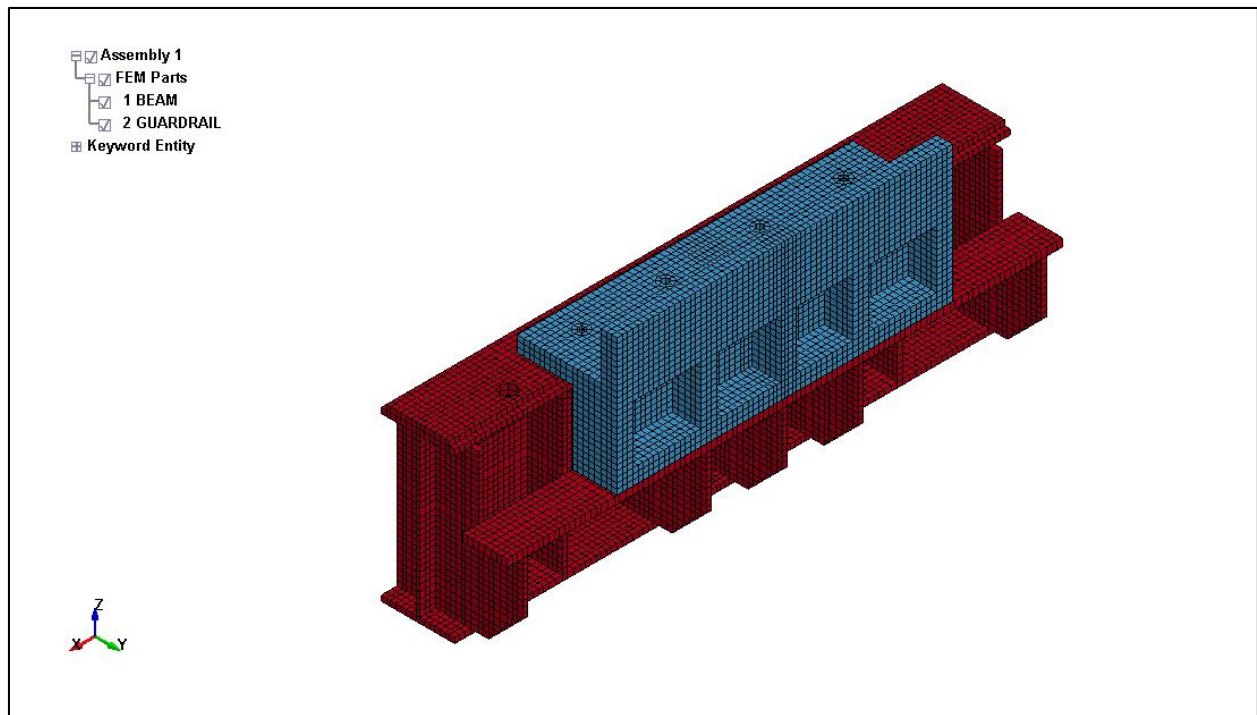
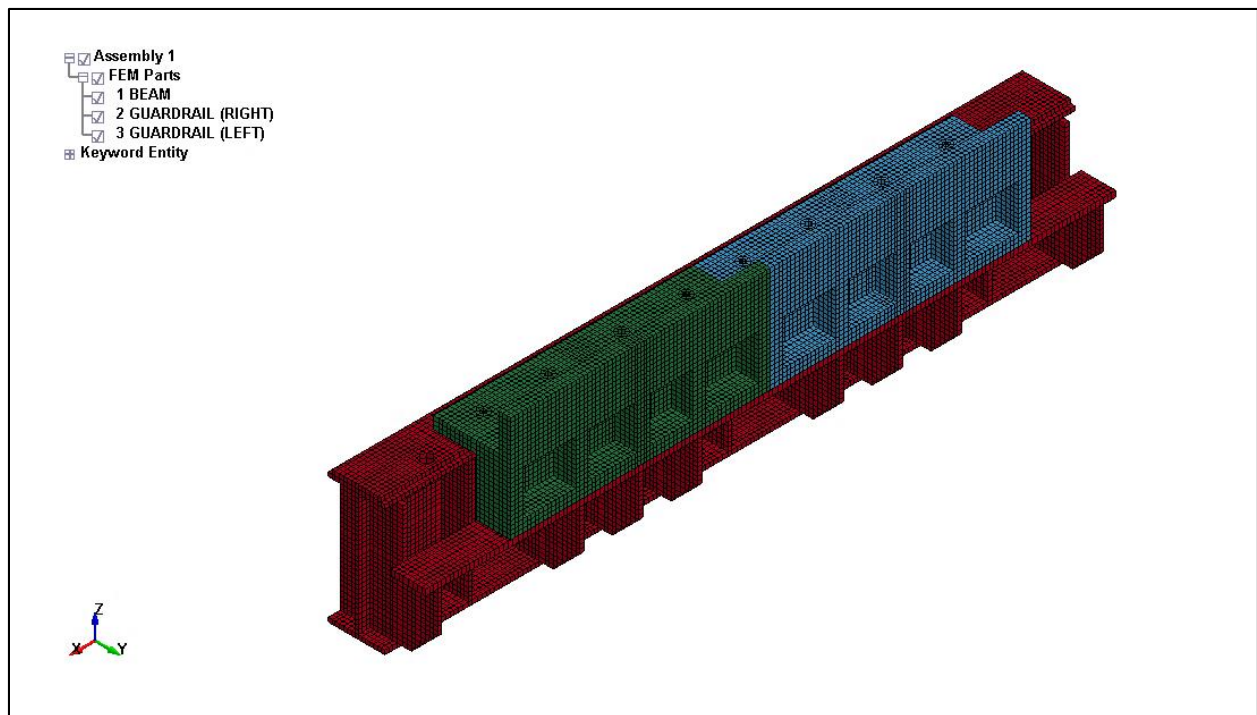Figure 11.   **Parts and Assembly: FEM-1 to FEM-4. (Part ID's are as shown.)**

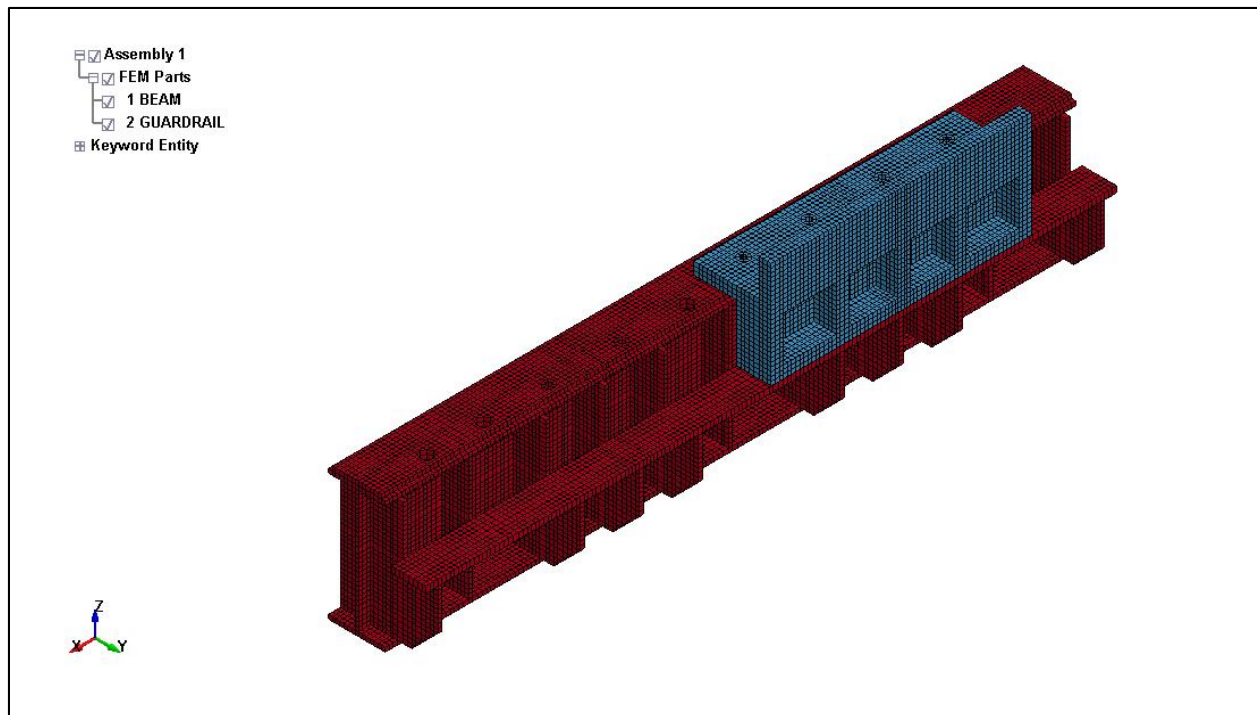Figure 12.   **Parts and Assembly: FEM-5. (Part ID's are as shown.)**

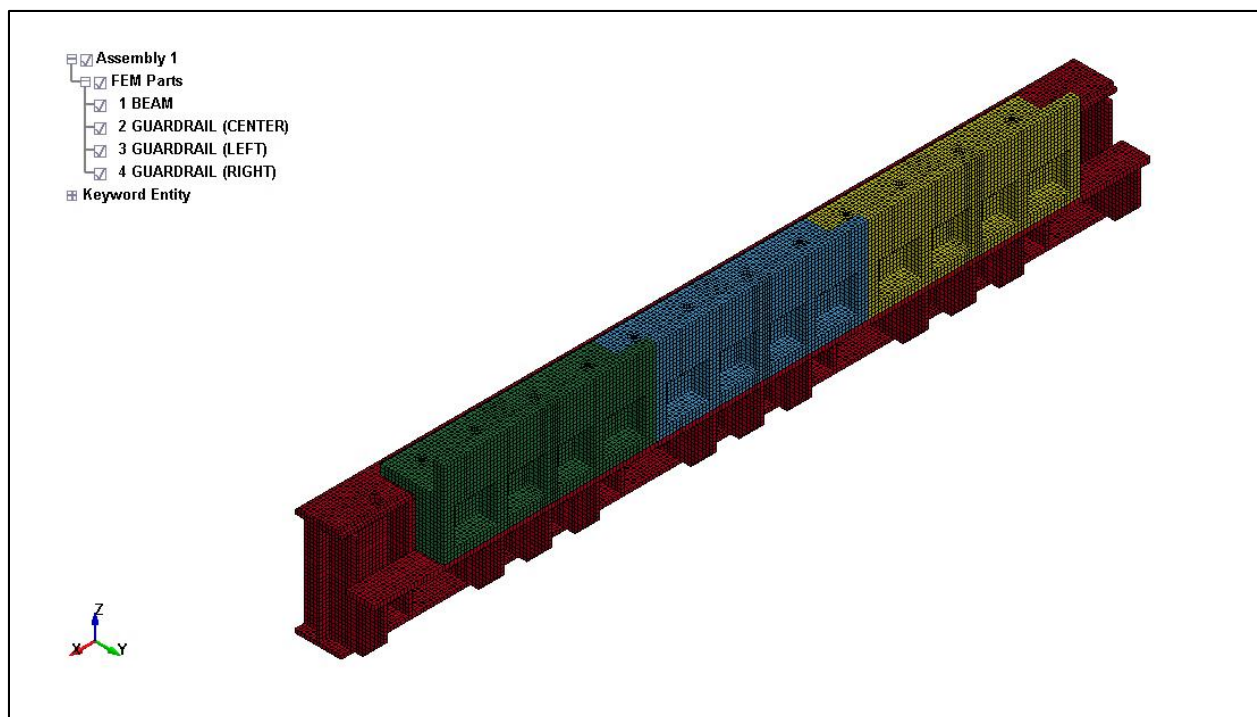Figure 13. **Parts and Assembly: FEM-6. (Part ID's are as shown.)**

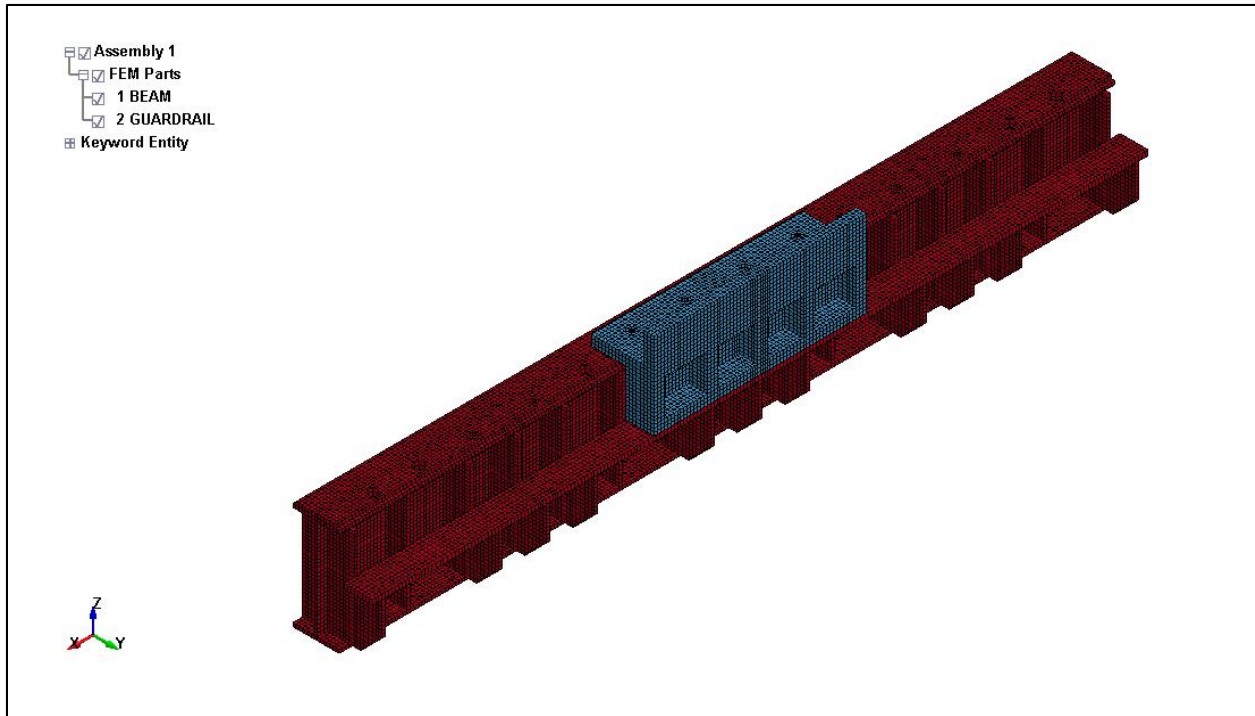Figure 14. **Parts and Assembly: FEM-7. (Part ID's are as shown.)**

Figure 15.   **Parts and Assembly: FEM-8. (Part ID's are as shown.)**

3.1.4 Boundary Conditions

Across all models, *global boundary constraint planes* and *nodal single point constraints* are used to define the boundary conditions. The use of these constraints is described below, and the boundary condition application for model FEM-1 to FEM-8 is presented in Figure 16 to Figure 18. [R.7]

It should be noted models FEM-1 to FEM-4 have identical boundary conditions as these models are all based on a 32-inch cross-beam spacing. Similarly, models FEM-5 and FEM-6 have identical boundary conditions (based on a 64-inch cross-beam spacing), as do models FEM-7 and FEM-8 (based on a 96-inch cross-beam spacing).

3.1.4.1 Global Boundary Constraint Plane

Global constraint planes are defined in the xy-direction at the underside of the beam segments to constrain translation in the z-direction. This accounts for the fact that

the beam segments modelled cannot penetrate through the platform modules on which they bear (platform modules are shown in Figure 1).

3.1.4.2 Nodal Single Point Constraints

As shown in the previous section, only a segment of the platform beam is included in the modeled assemblies. The portion of the platform beam not modelled is replaced with a set of nodal single point constraints to the beam segment ends to constrain translation in the x-direction (along the beam axis).

Similarly, the platform module's cross-beams are not modelled and are instead replaced by a set of nodal single point constraints applied to constrain the beam/cross-beam interface against translation in the y-direction (along the cross-beam axis).

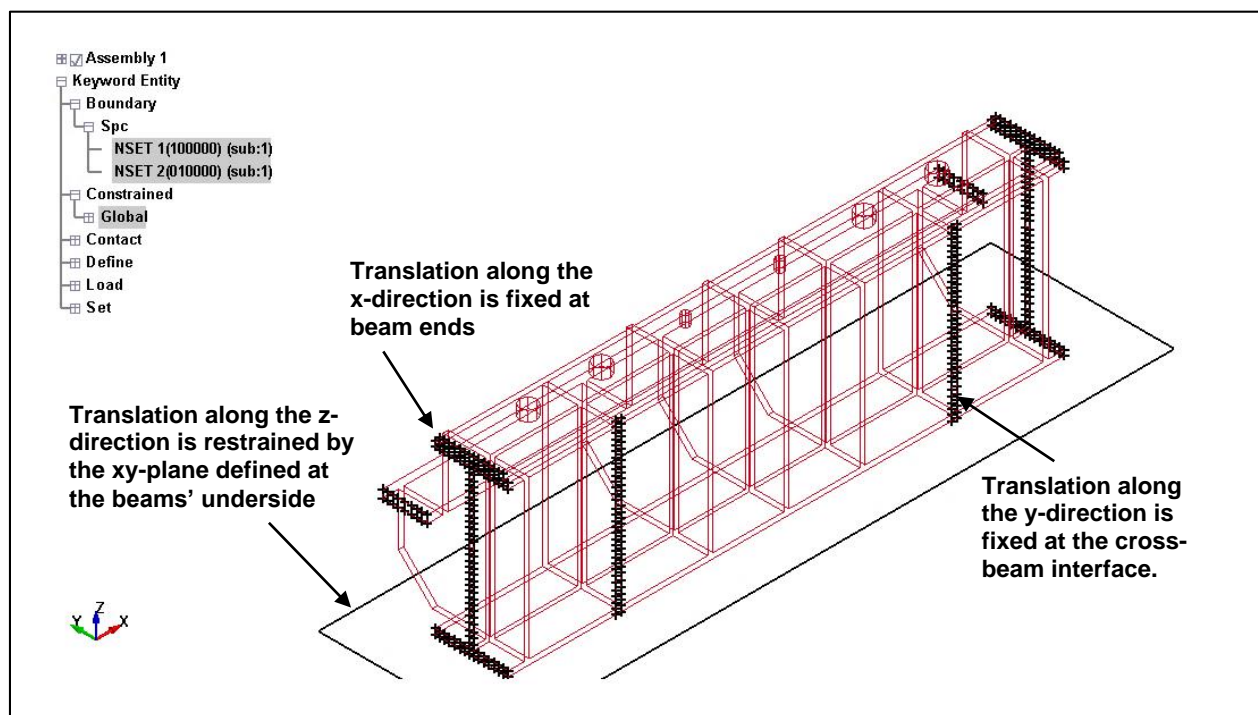### 3.1.4.3 Boundary Condition Application

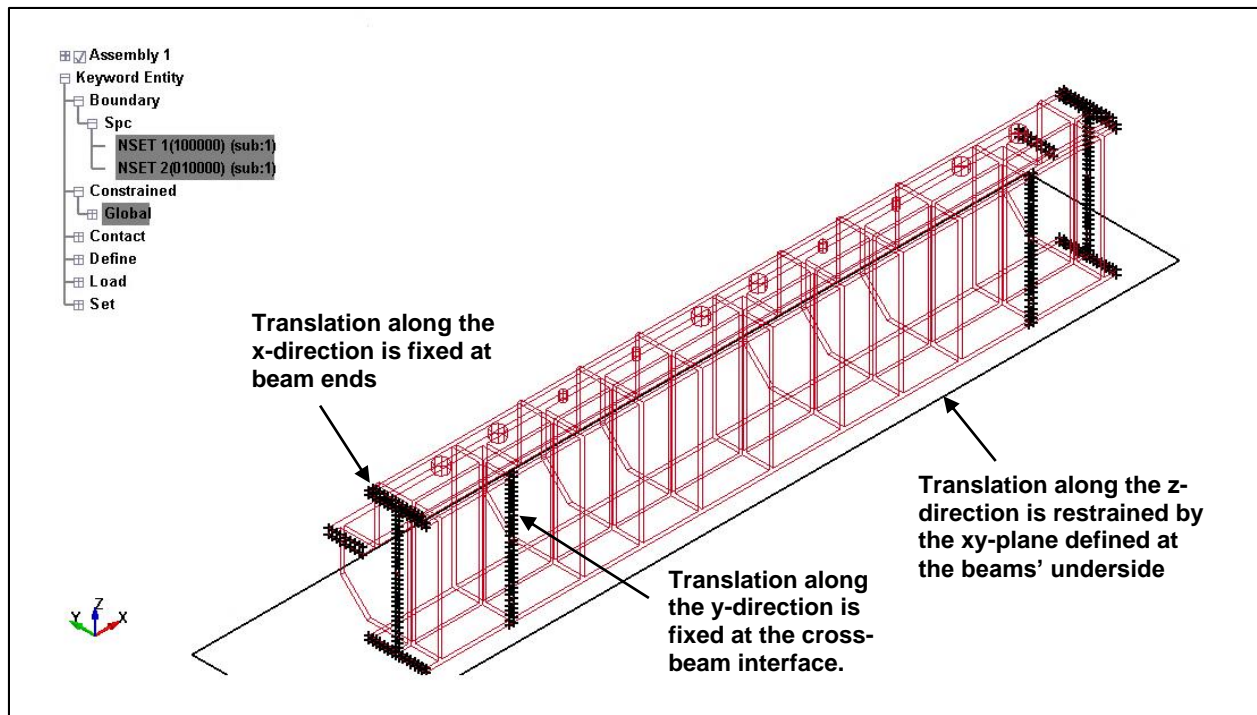Figure 16. **Boundary Conditions: FEM-1 to FEM-4.**
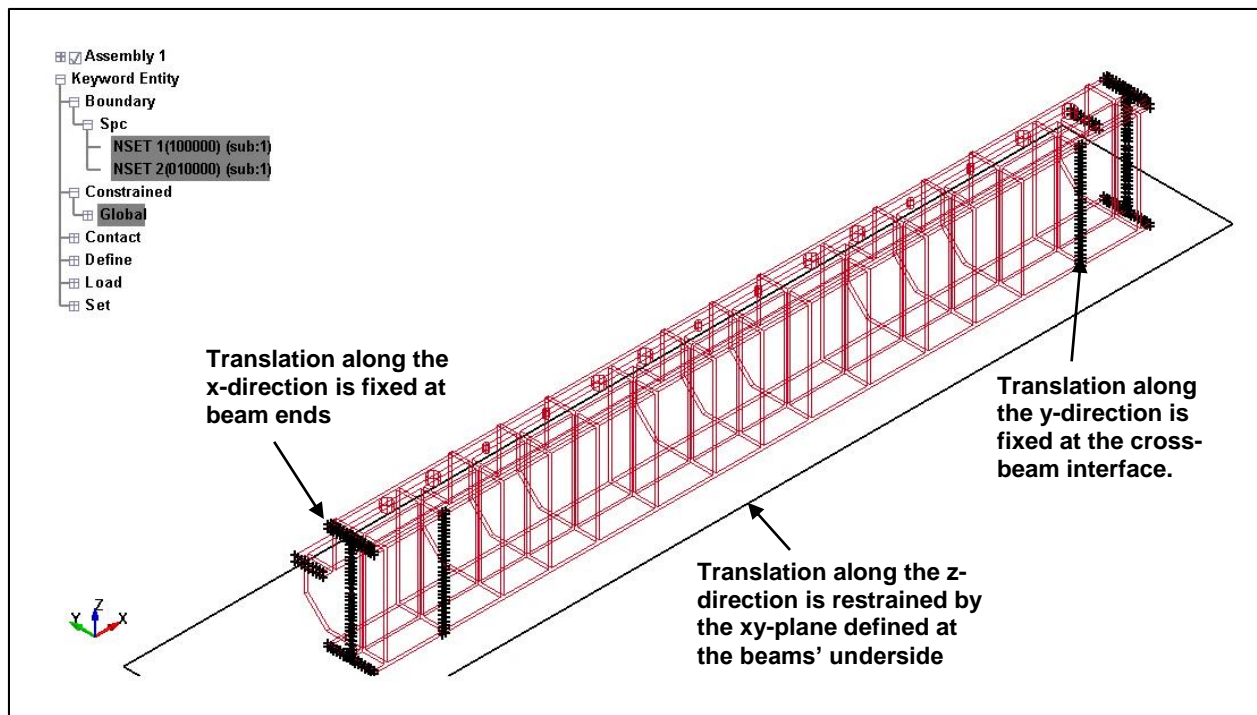
Figure 17. **Boundary Conditions: FEM-5 and FEM-6.**

Figure 18. **Boundary Conditions: FEM-7 and FEM-8.**

3.1.5 Materials

The beam segments and guardrail modules modelled are both made of structural grade mild carbon steel. In the models, two different material definitions are created based on the properties of carbon steel:

1. A plastic kinematic material definition is assigned to the beam segment. This material type provides a cost-effective model suitable for modelling isotropic materials such as steel. [R.7]
2. A rigid material definition is assigned to the guardrail modules. Analyzing guardrails as non-deformable rigid bodies significantly reduces the computational cost associated with the analysis and is justified by the assumption that failure of the guardrail to remain mounted after impact will be a result of deformation in the beam segment (and not the guardrail). [R.7]

The material definitions used in the model are presented in Table 4.

Table 4. **Material definitions.**

Material ID	1	2	
Type	Plastic kinematic	Rigid	
Assigned	Beam segments	Guardrail modules	
Mass Density	7.350e-004	7.350e-004	$(lbf\text{-}s^2/in)/in^3$
Young's Modulus	2.900e+007	2.900e+007	psi
Poisson's Ratio	0.3	0.3	
Yield Stress	5.000e+004	n/a	psi
Tangent Modulus	2.900e+006	n/a	psi

3.1.6 Loading

Two types of load definitions are used in the models; *body loads* are used to apply the self-weight resulting from gravity on the assembly, and n*ode loads* are used to apply the RGV impact load on a particular node (or set of nodes) as required to model the impact scenarios considered in this study.

While body load definitions are identical across all models (a gravitational acceleration of 386.4 in/sec^2 is applied downwards along the z-axis), the nodal loads defined vary from one model to another to model the various impact orientations and impact locations considered. The nodal loads defined for each model are described and presented in Section 3.1.6.1 to Section 3.1.6.8 and in Figure 20 to Figure 27, respectively.

It should be noted that while nodal loads are defined in terms of location (node ID) and magnitude, LS-DYNA also requires that a *load curve* be defined to describe the load variation through time. As the RGV will failsafe by self-disabling when impact is detected, it is assumed that impact loads will peak 0.1 seconds after impact and decrease to 0 at 0.2 seconds as shown in Figure 19, where abscissa values represent time (in seconds) and ordinate values represent load magnitude multipliers). [R.7]
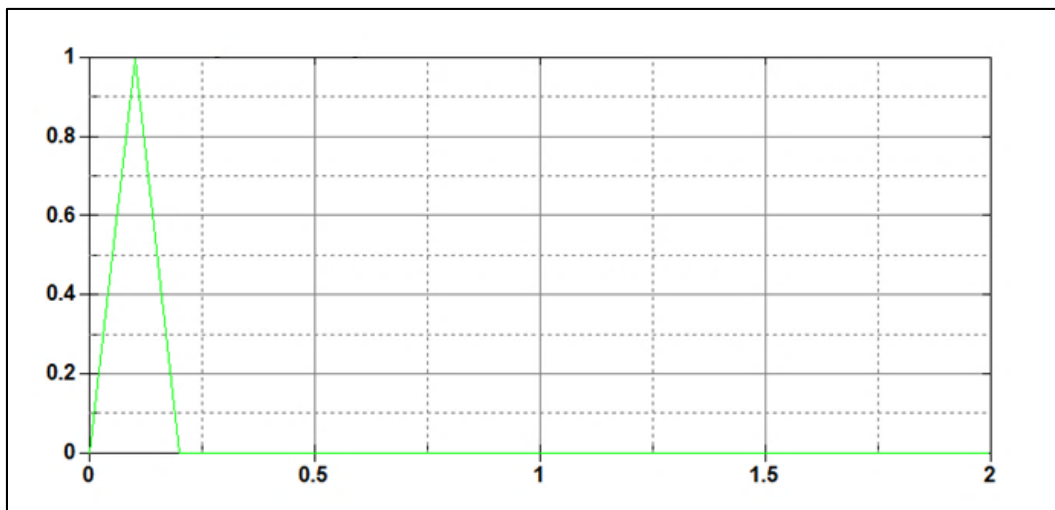

Figure 19.   **Load Curve: FEM-1 to FEM-8.**

24

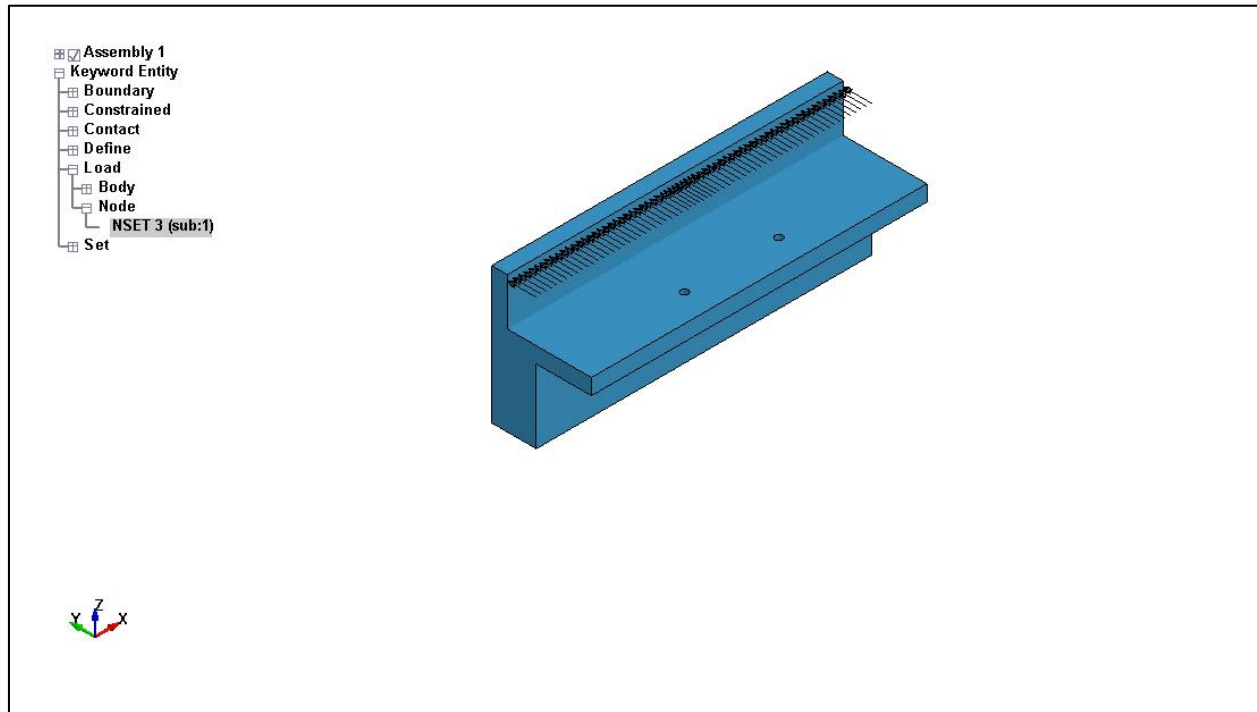3.1.6.1 <u>FEM-1 Loading</u>

Figure 20. **Load Application: FEM-1.**

Model FEM-1 is associated with a head-on impact scenario as described in Table 2. This implies that the RGV frame will come in full contact with the guardrails and impose a uniformly distributed load at the frame-guardrail interface.

Dividing the RGV impact load (45,000 lbf) by the width of the RGV frame (79 inches) yields a uniformly distributed load of 570 lbf/in. This load is applied on the guardrail module in the y-direction at a height of 4 inches above the working surface, coinciding with nominal drive height of the lowest part of the RGV frame.

The load application for FEM-1 is shown above in Figure 20. The beam segment is hidden in the figure for clarity.
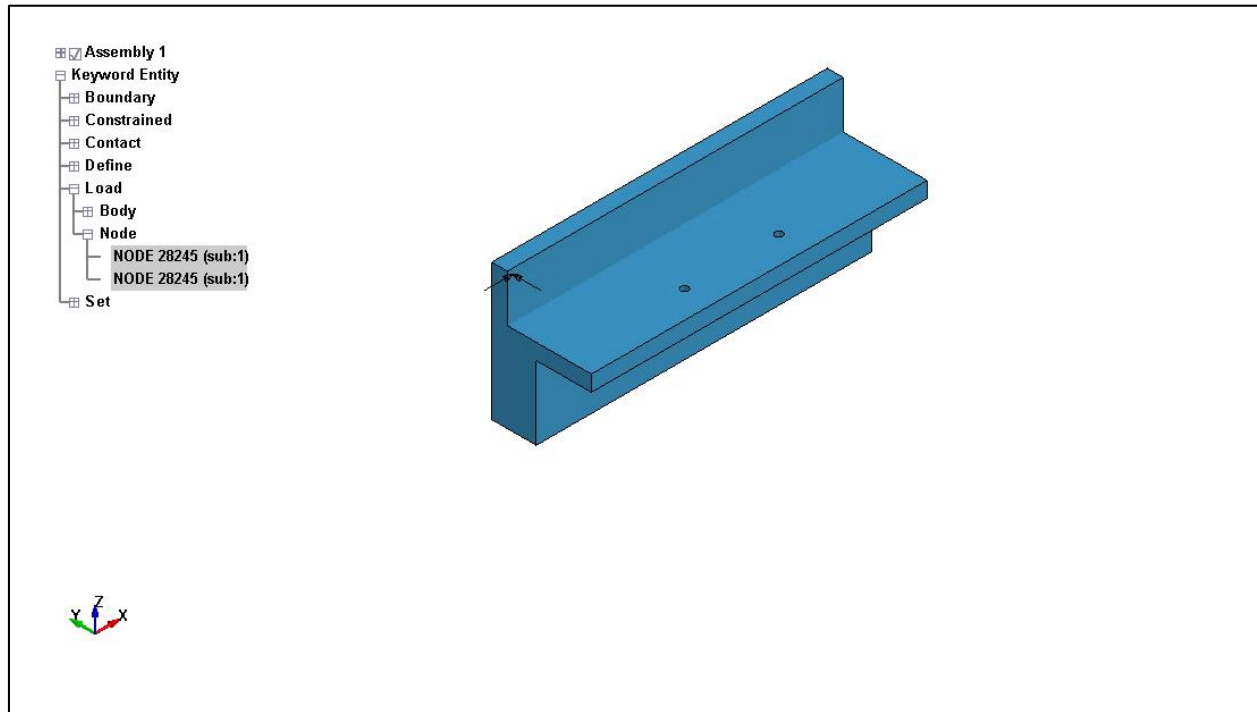
3.1.6.2 FEM-2 Loading

Figure 21. **Load Application: FEM-2.**

Model FEM-2 is associated with a side impact scenario as described in Table 2. This implies that only the corner of the RGV frame will come in contact with the guardrail module, imposing a concentrated load at the frame-guardrail interface.

Since an impact orientation of 60º is considered, the RGV impact load (45,000 lbf) is resolved into two orthogonal components, yielding concentrated loads of 22,500 lbf and 39,000 lbf along the x- and y-axes, respectively.

These loads are applied at the left-hand side of the module at a height of 4 inches above the working surface, coinciding with nominal drive height of the lowest part of the RGV frame.

The load application for FEM-2 is shown above in Figure 21. The beam segment is hidden in the figure for clarity.
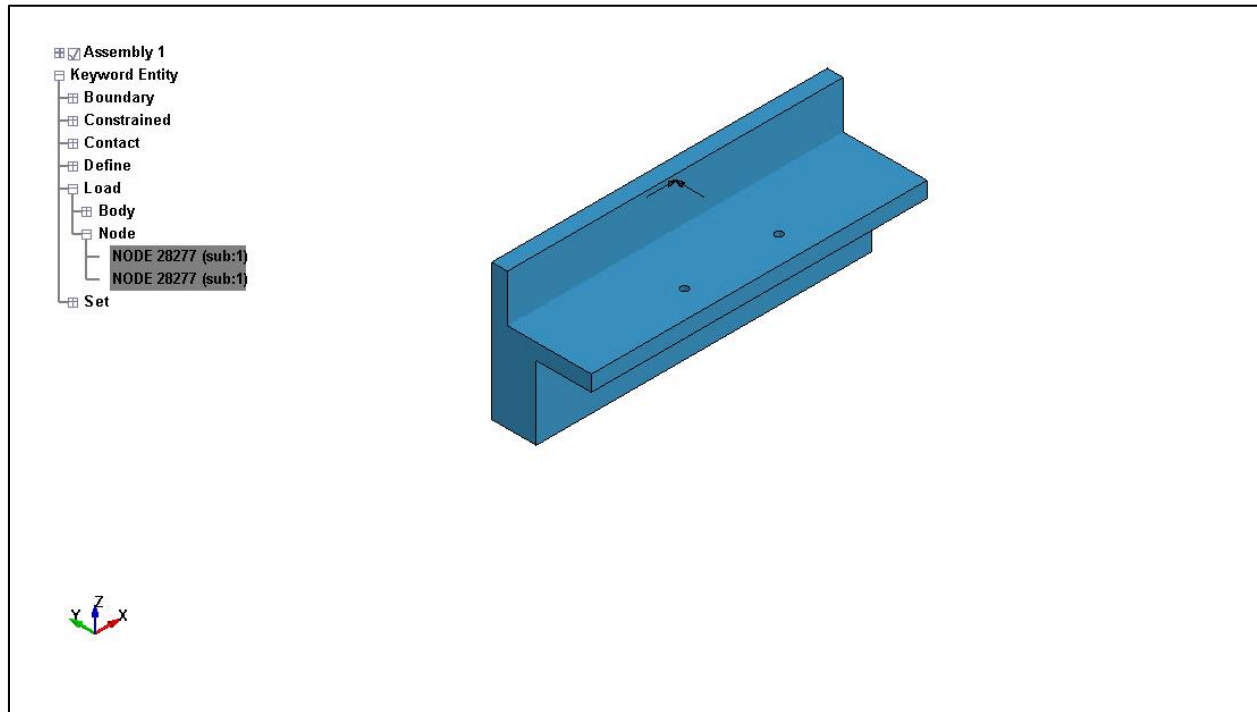
3.1.6.3 FEM-3 Loading

Figure 22. **Load Application: FEM-3.**

Model FEM-3 is associated with a side impact scenario as described in Table 2. The load application is similar to model FEM-2 (description provided in Section 3.1.6.2) with the difference being that the load is applied at the center of the guardrail module.

The load application for FEM-3 is shown above in Figure 22. The beam segment is hidden in the figure for clarity.
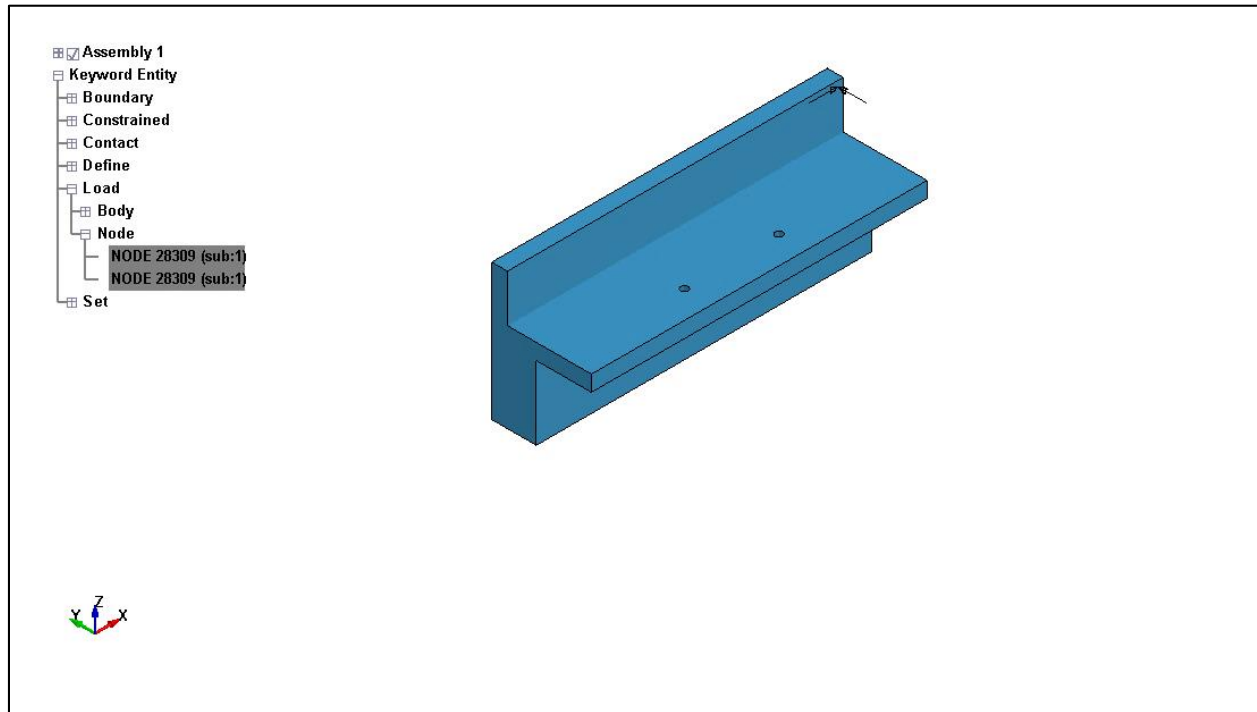
3.1.6.4 FEM-4 Loading

Figure 23.   **Load Application: FEM-4.**

Model FEM-4 is associated with a side impact scenario as described in Table 2. The load application is similar to model FEM-2 (description provided in Section 3.1.6.2) with the difference being that the load is applied at the right-hand side of the guardrail module.

The load application for FEM-4 is shown above in Figure 23. The beam segment is hidden in the figure for clarity.
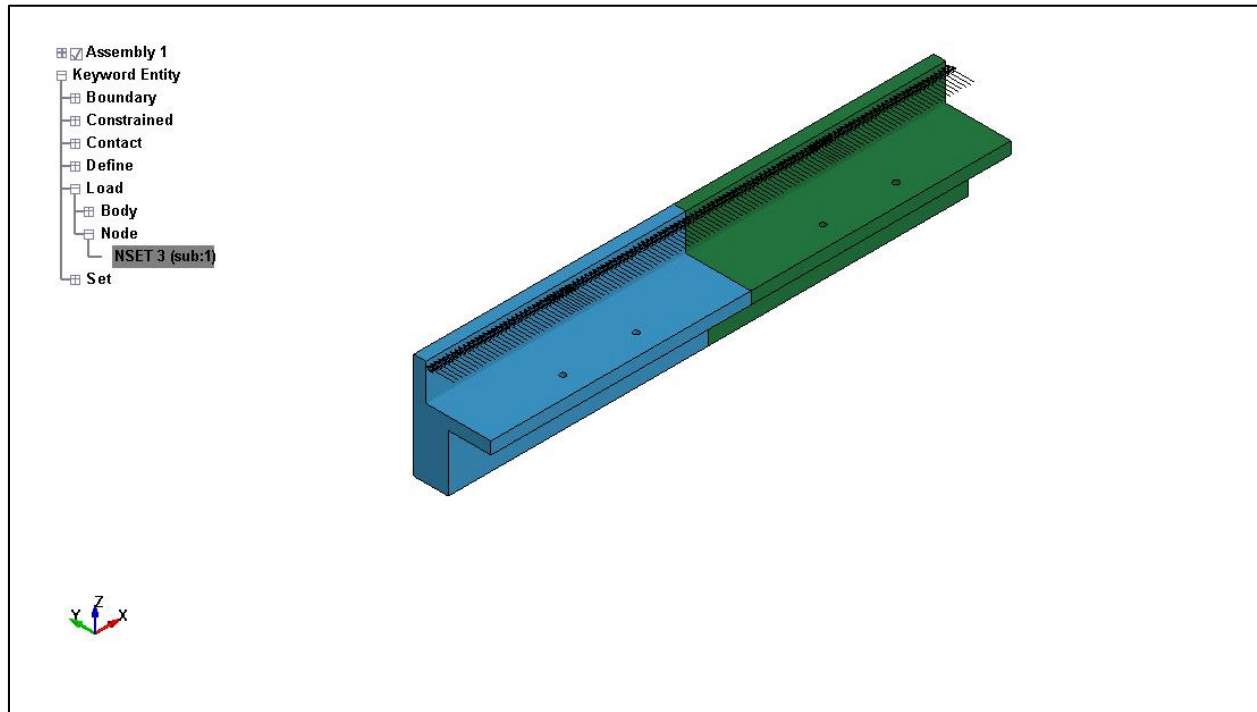
3.1.6.5 <u>FEM-5 Loading</u>

Figure 24. **Load Application: FEM-5.**

Model FEM-5 is associated with a head-on impact scenario as described in Table 2. The load application is similar to model FEM-1 (description provided in Section 3.1.6.1) with the difference being that the load is applied on two guardrail modules instead of one.

The load application for FEM-5 is shown above in Figure 24. The beam segment is hidden in the figure for clarity.
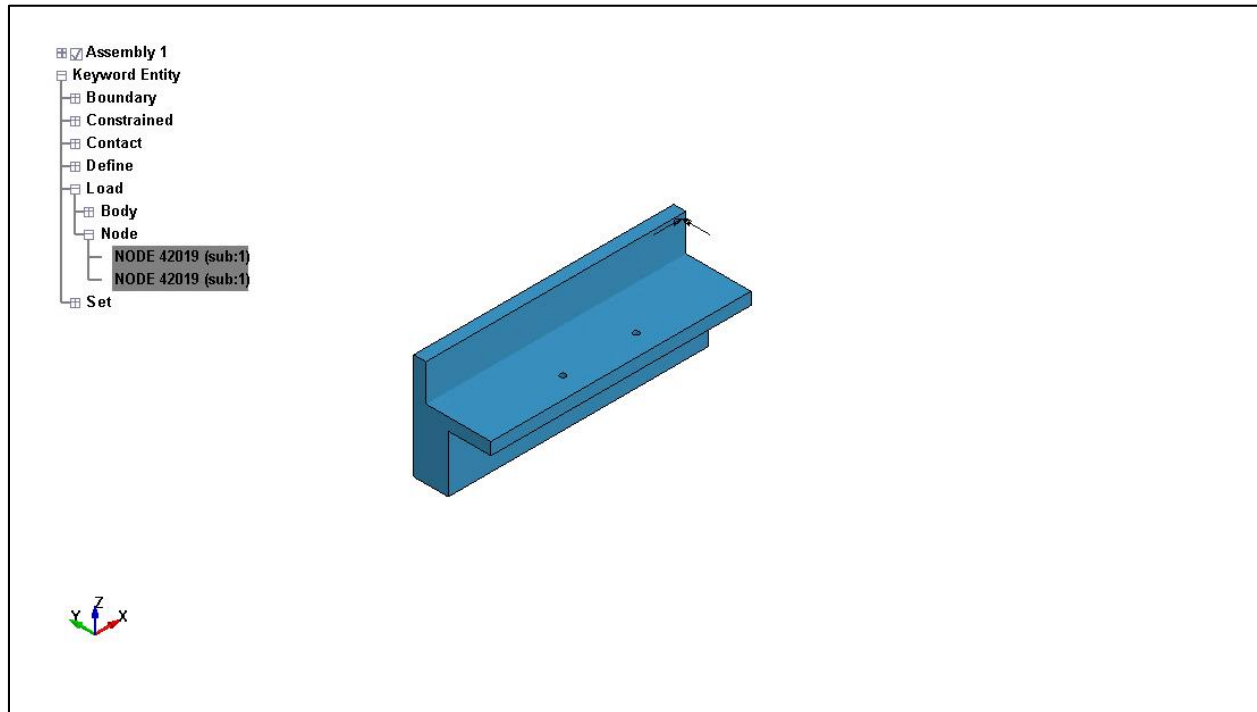
3.1.6.6 FEM-6 Loading

Figure 25. **Load Application: FEM-6.**

Model FEM-6 is associated with a side impact scenario as described in Table 2. The load application is similar to model FEM-2 (description provided in Section 3.1.6.2) with the difference being that the load is applied at the right-hand side of the guardrail module.

It should be noted that in this case, the right-hand side of the guardrail module coincides with the center of the beam segment having a 64-inch cross-beam spacing, which is where the impact is considered to take place.

The load application for FEM-6 is shown above in Figure 25. The beam segment is hidden in the figure for clarity.

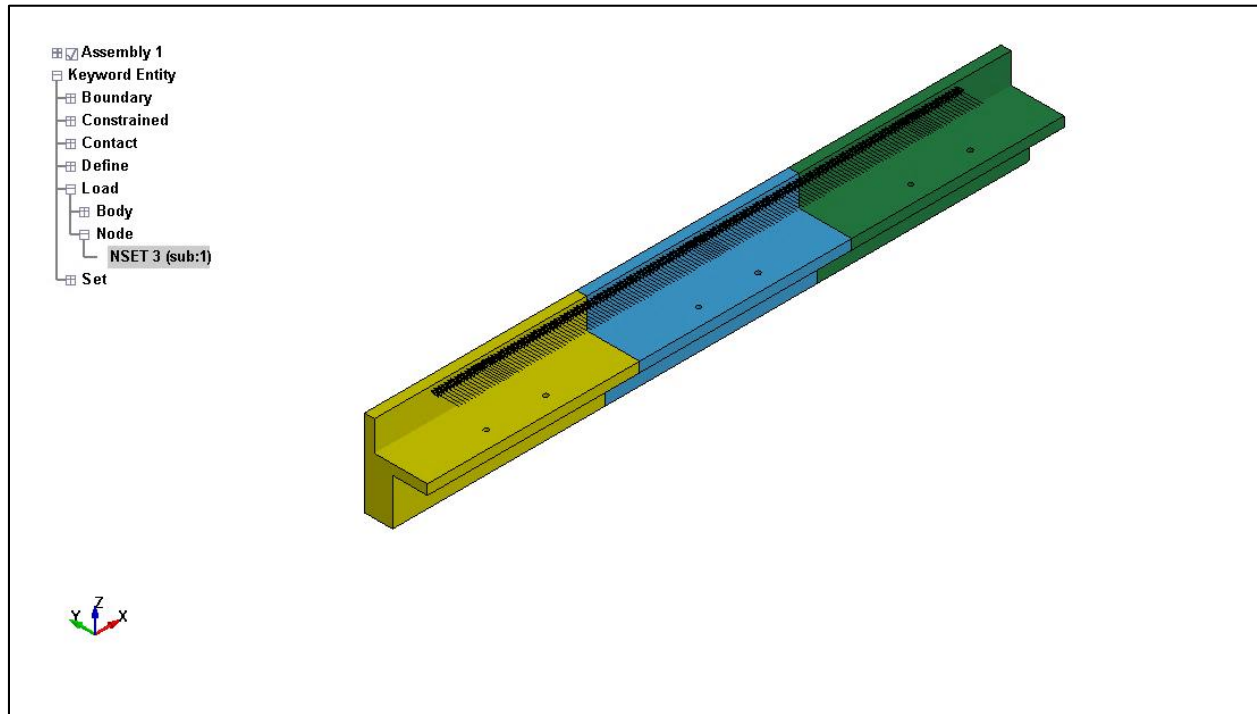3.1.6.7 <u>FEM-7 Loading</u>

Figure 26. **Load Application: FEM-7.**

Model FEM-7 is associated with a head-on impact scenario as described in Table 2. The load application is similar to model FEM-1 (description provided in Section 3.1.6.1) with the difference being that the load is applied across a 79-inch width spanning three guardrail modules.

The load application for FEM-7 is shown above in Figure 26. The beam segment is hidden in the figure for clarity.
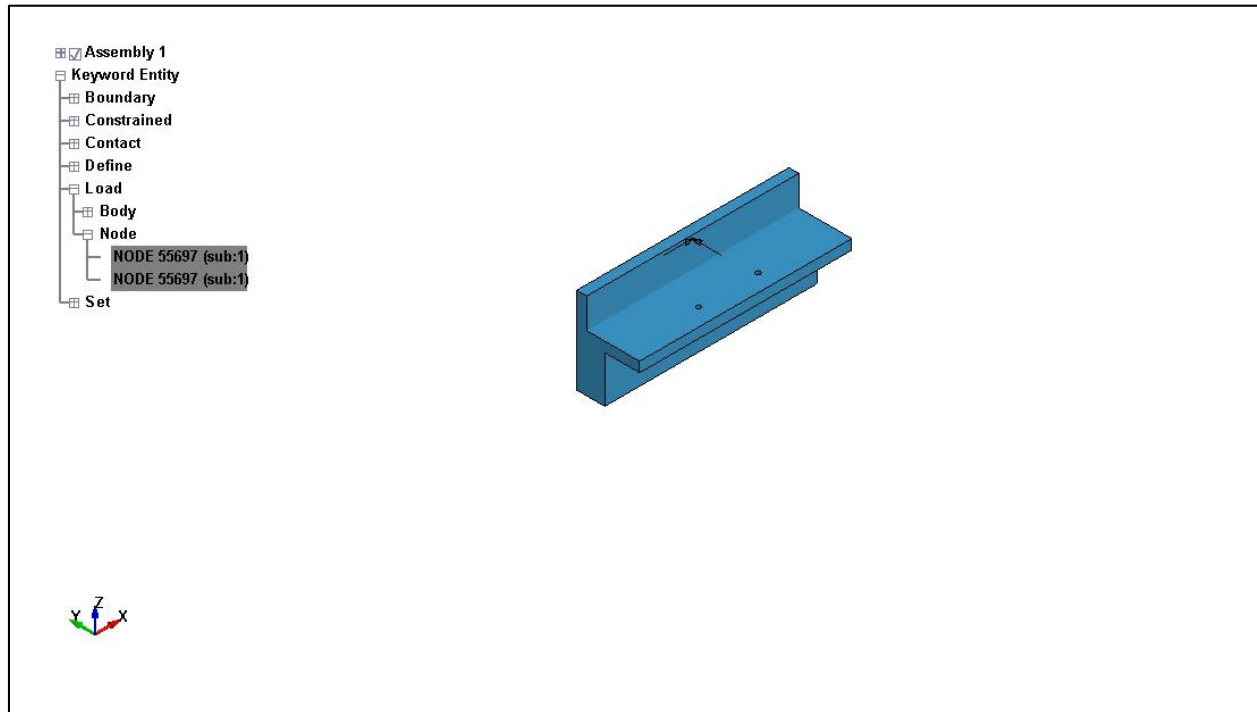
3.1.6.8 FEM-8 Loading

Figure 27. **Load Application: FEM-8.**

Model FEM-8 is associated with a side impact scenario as described in Table 2. The load application is similar to model FEM-2 (description provided in Section 3.1.6.2) with the difference being that the load is applied at the center of the guardrail module.

It should be noted that in this case, the center of the guardrail module coincides with the center of the beam segment having a 96-inch cross-beam spacing, which is where the impact is considered to take place.

The load application for FEM-8 is shown above in Figure 27. The beam segment is hidden in the figure for clarity.

3.1.7 Analysis Settings

The analysis settings described in this section are common across all models.

3.1.7.1 Contact Settings

Automatic surface-to-surface contact commands are used to define the contact interface between the guardrail modules and beam segments, and to initiate the contact-impact algorithm described in Section 2.2.3. The contact commands are defined with the settings presented in Table 5.

Table 5. **Contact Settings.**

Slave	Guardrail modules
Master	Beam segment
Static Coefficient of Friction	0.2
Dynamic Coefficient of Friction	0.2

3.1.7.2 Database Settings (Output Files)

Database settings are used to specify the output format as well as the time interval between output states. The *d3plot* format is selected and an output state interval of 0.1 seconds is specified. This causes the geometry and state variables to be stored into output files at 0.1 second intervals, allowing deformed shapes and element stresses to be plotted and animated. [R.7]

3.1.7.3 Time Control Settings

Time control commands are used to specify the termination time for the analysis. After making trial runs with various termination times, a termination time of 0.5 seconds was selected as it was found to capture a sufficient amount of the impact response for evaluating the performance of the guardrails.

3.2 Results and Discussion

In accordance with the methodology set out in Section 1.3.1, the von Mises stresses and deformed shapes for each guardrail/beam assembly were obtained from the LS-DYNA output to evaluate the performance of the guardrails with the bolts removed. The evaluation is achieved by comparing the output from LS-DYNA against the following acceptance criteria:

1. The von Mises stresses obtained shall not exceed the yield criterion, taken as 45,000 psi, during impact.
2. The deformed shapes shall demonstrate that the guardrail modules remain mounted and do not unlatch upon impact.

The stress plots and deformed shapes obtained for each model are presented below in Sections 3.2.1 and 3.2.2, and a discussion of the results follows in Section 3.2.3.

It should be noted that while the deformed shapes are presented at each output state (i.e. t=0.0 through t=0.5), the stress plots are provided only at the time of impact (i.e. t=0.1) where the maximum stresses were observed to occur.
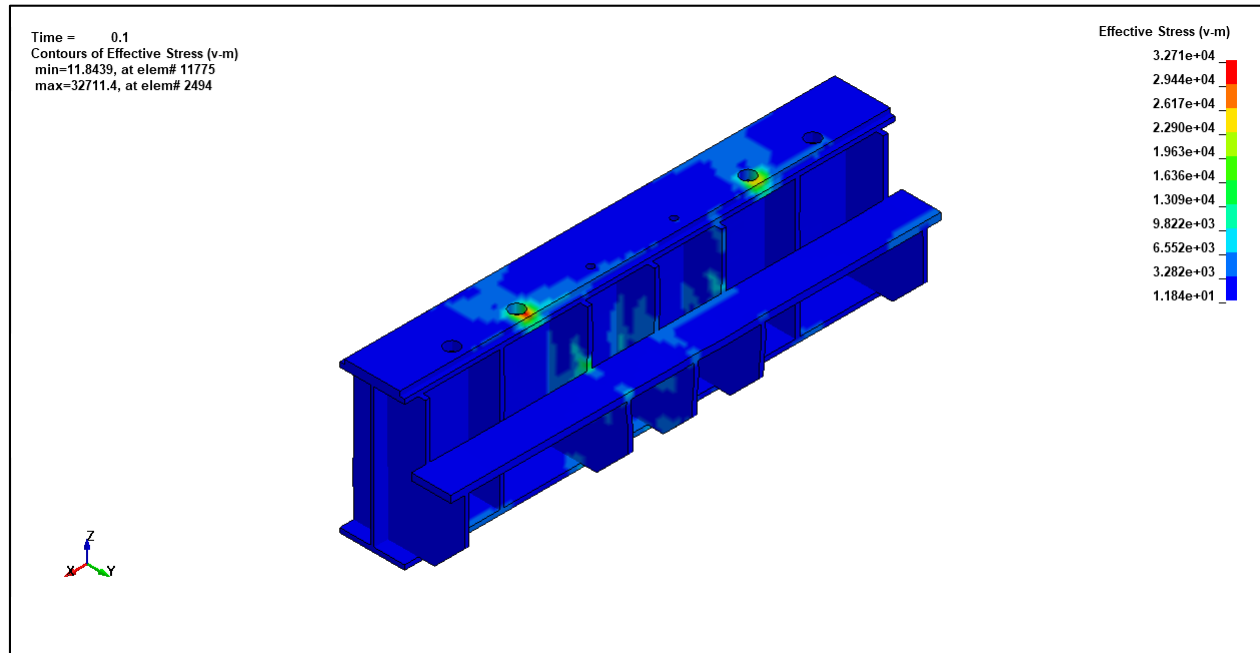
3.2.1 Von Mises Stresses
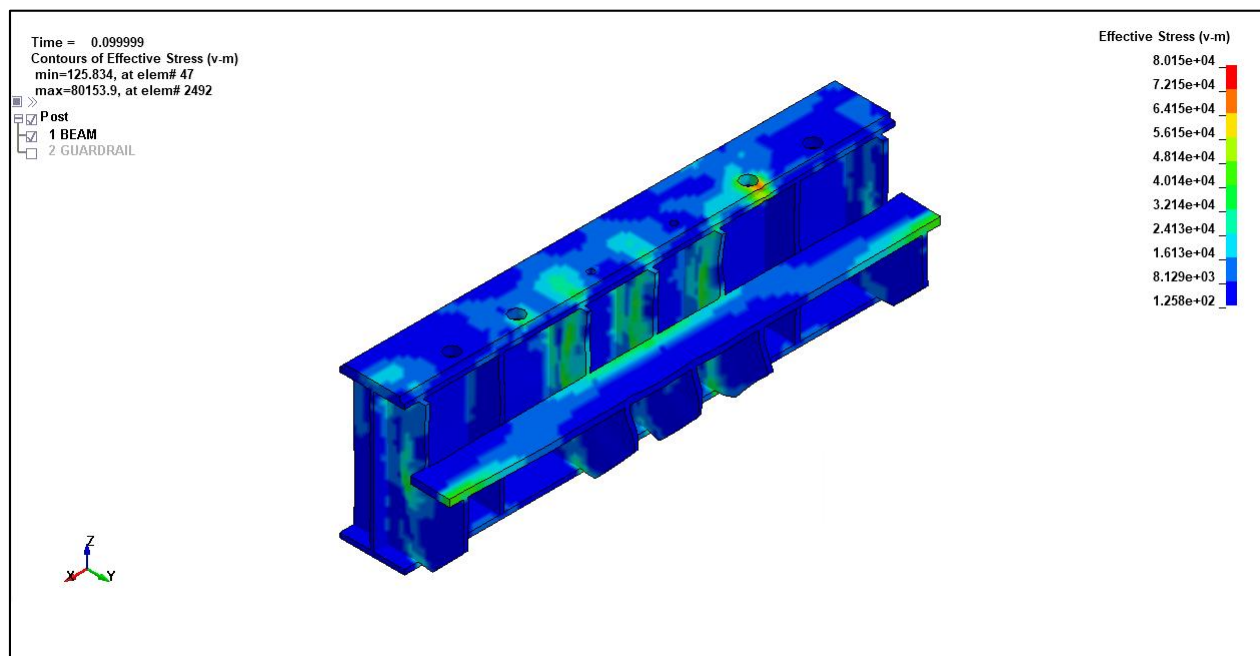

Figure 28.   **Von Mises Stress Plot: FEM-1. (t=0.1)**

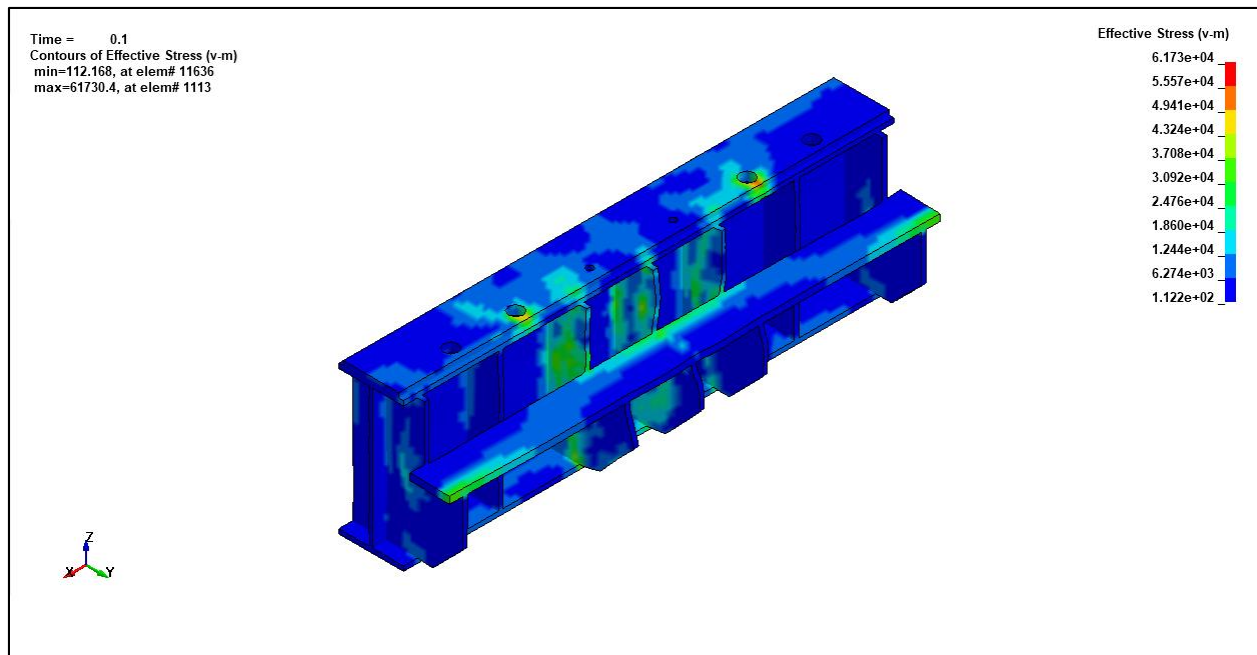

Figure 29.   **Von Mises Stress Plot: FEM-2. (t=0.1)**

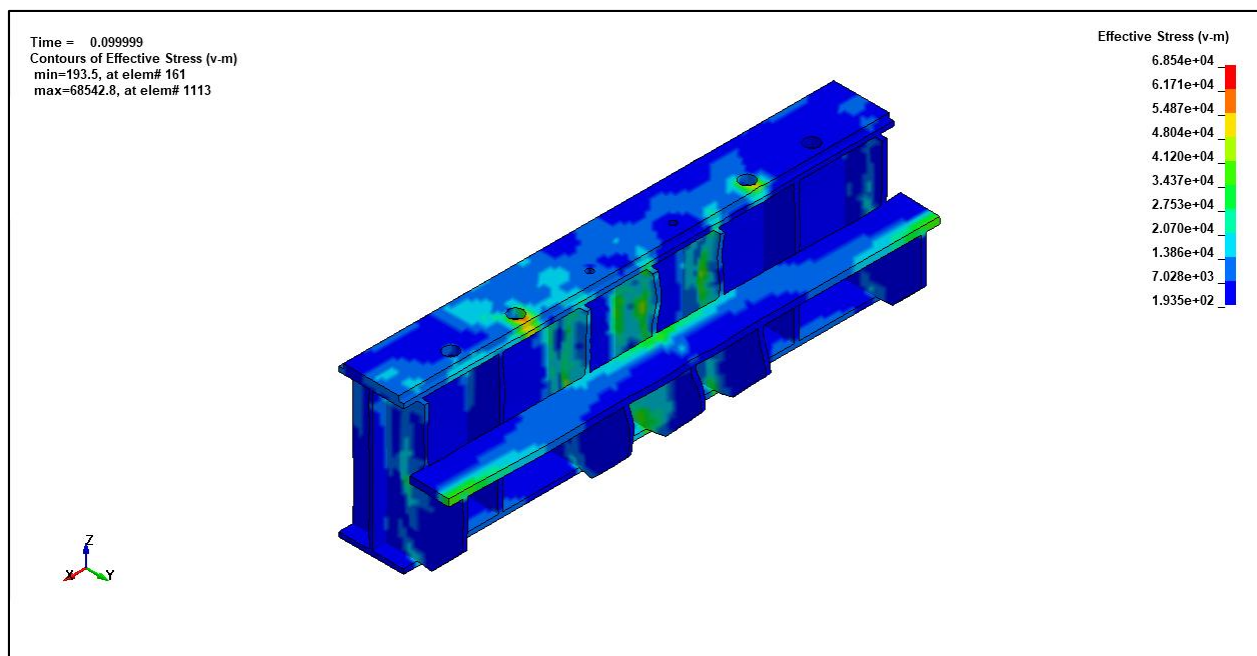Figure 30.   **Von Mises Stress Plot: FEM-3. (t=0.1)**

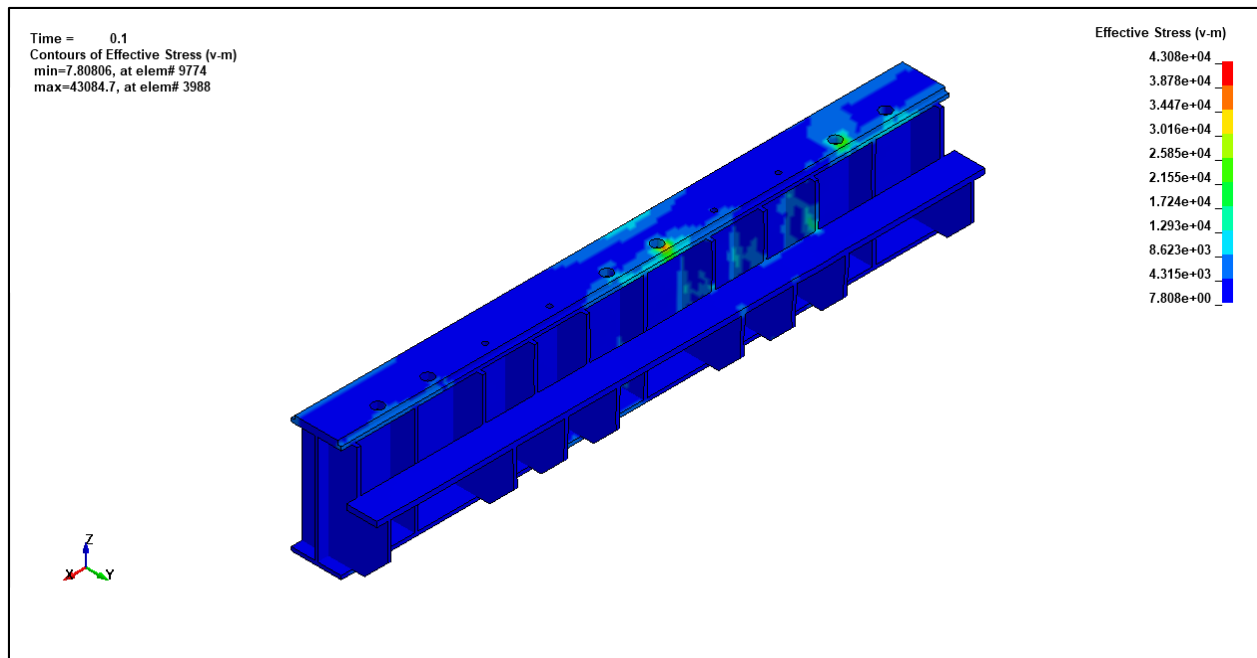Figure 31.   **Von Mises Stress Plot: FEM-4. (t=0.1)**

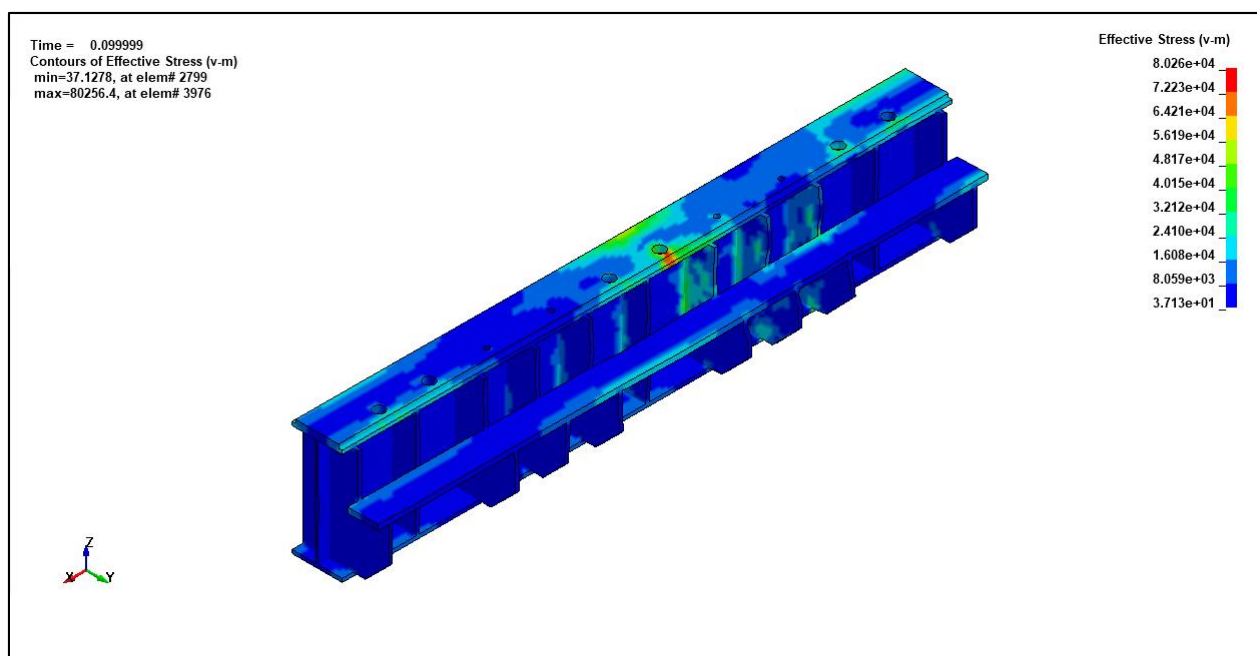Figure 32.   **Von Mises Stress Plot: FEM-5. (t=0.1)**
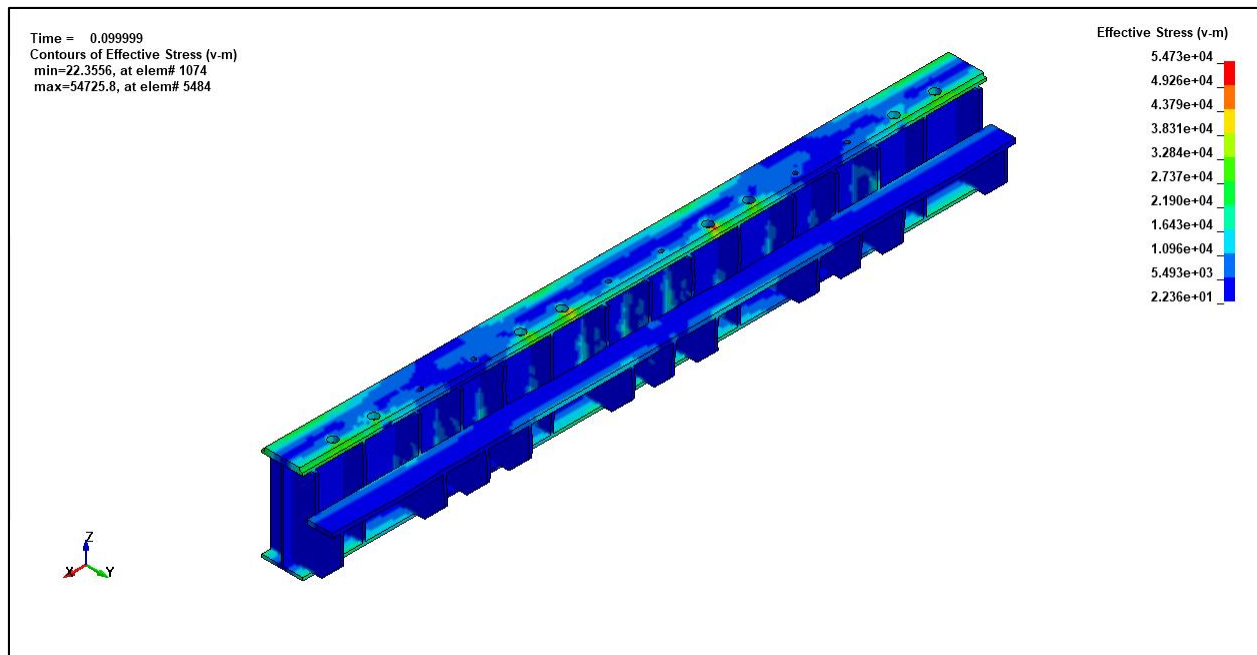

Figure 33.   **Von Mises Stress Plot: FEM-6. (t=0.1)**

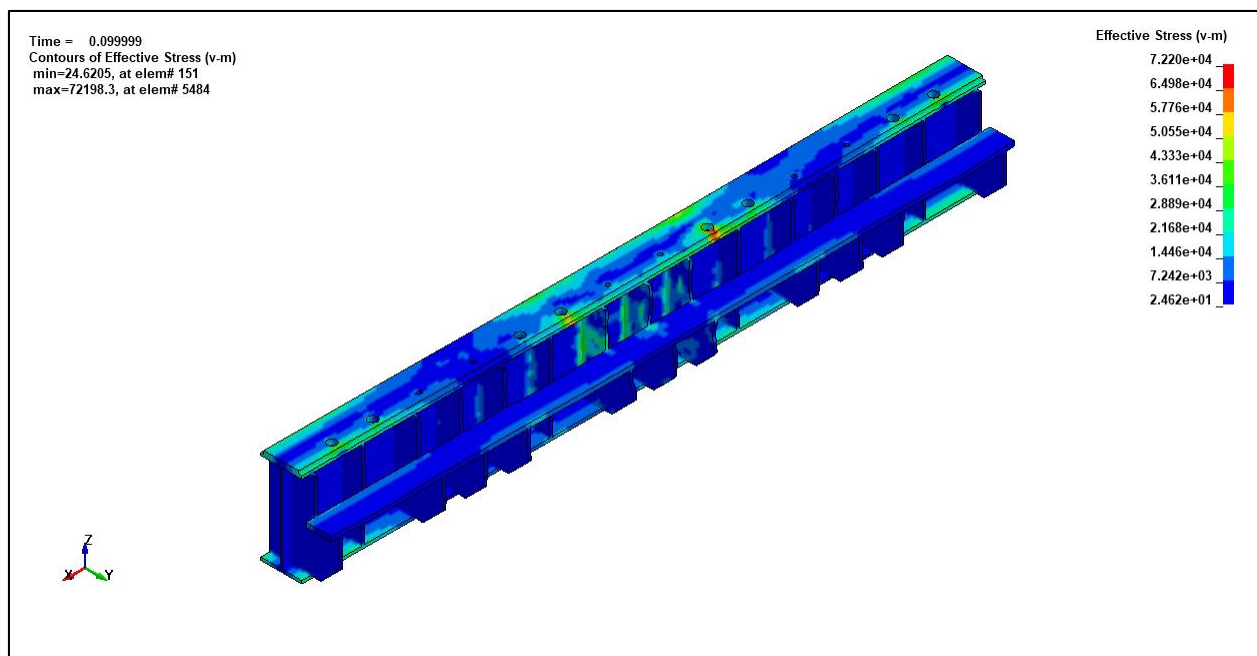Figure 34.   **Von Mises Stress Plot: FEM-7. (t=0.1)**

Figure 35.   **Von Mises Stress Plot: FEM-8. (t=0.1)**
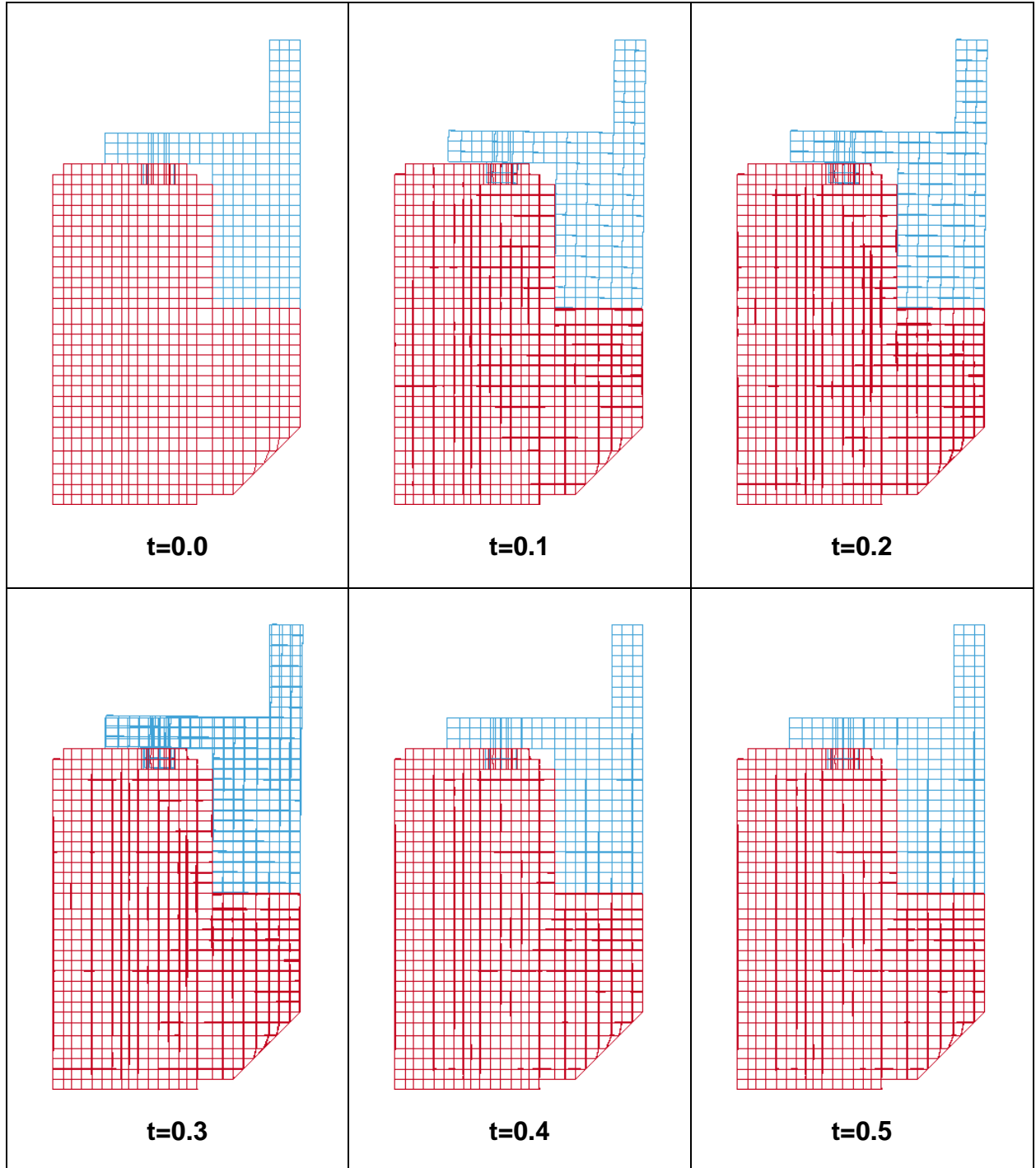
3.2.2 Deformed Shapes

Figure 36. **Deformed Shapes: FEM-1. (t=0.0 to t=0.5)**

Figure 37.   **Deformed Shapes: FEM-2. (t=0.0 to t=0.5)**

40
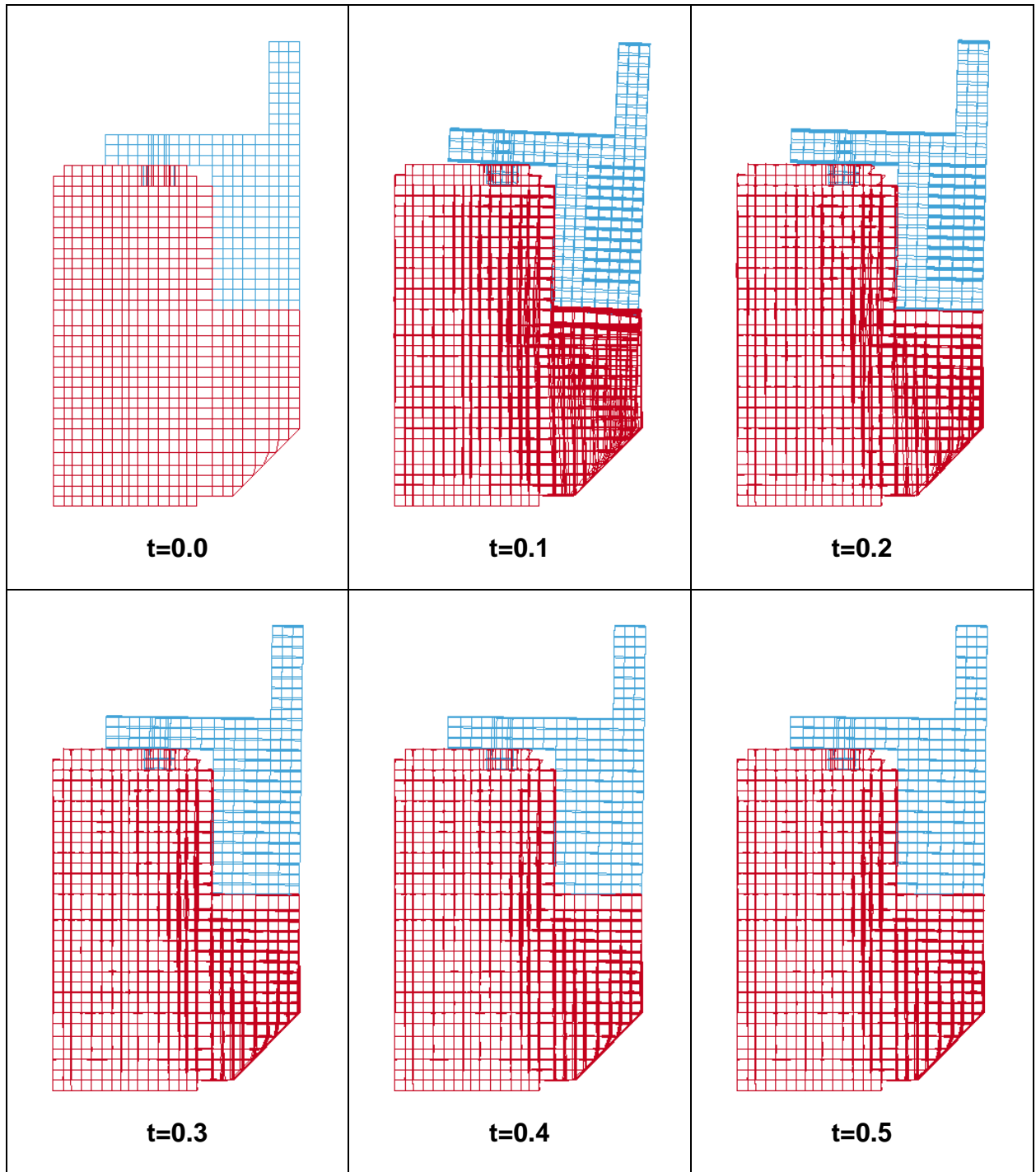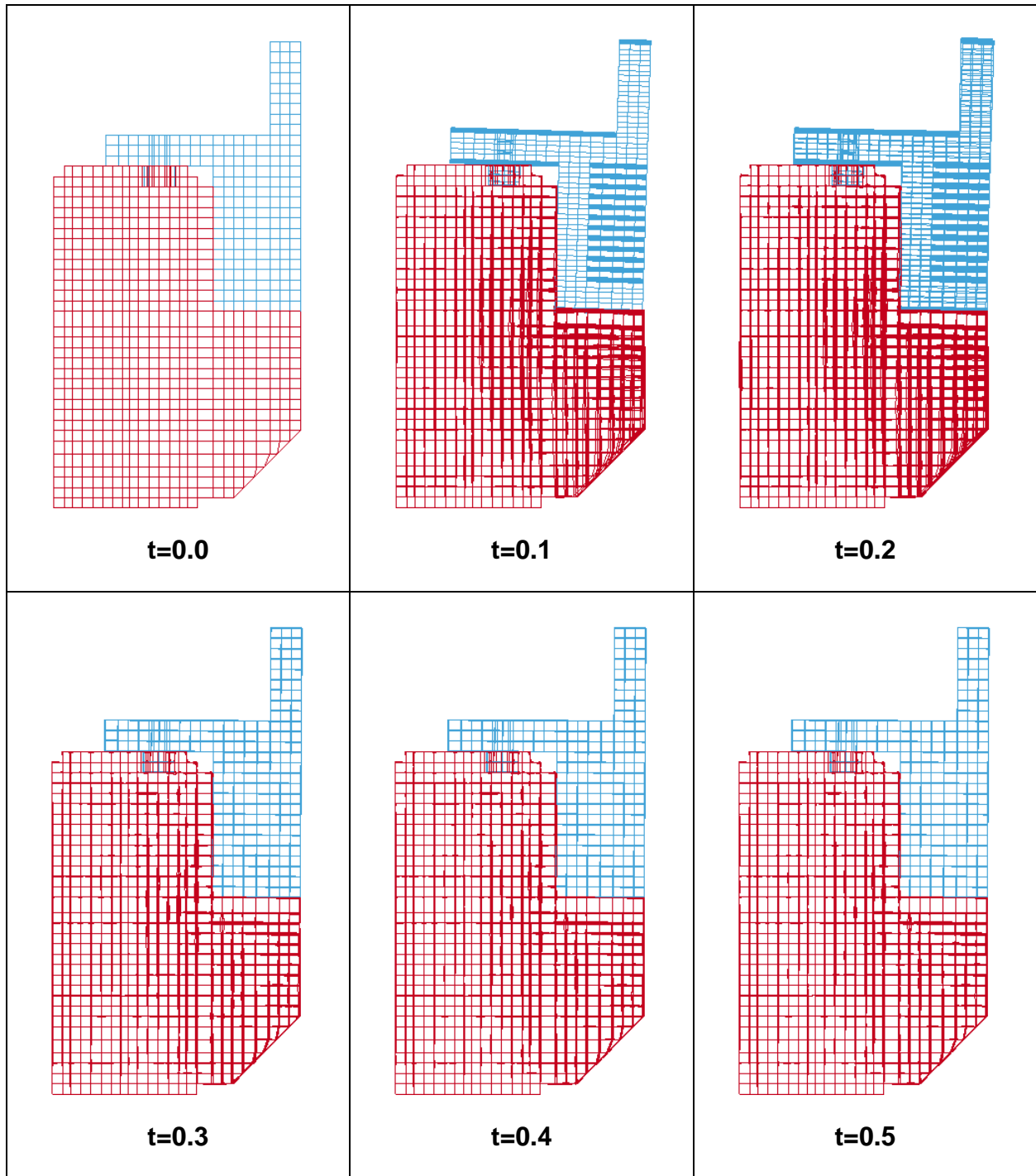
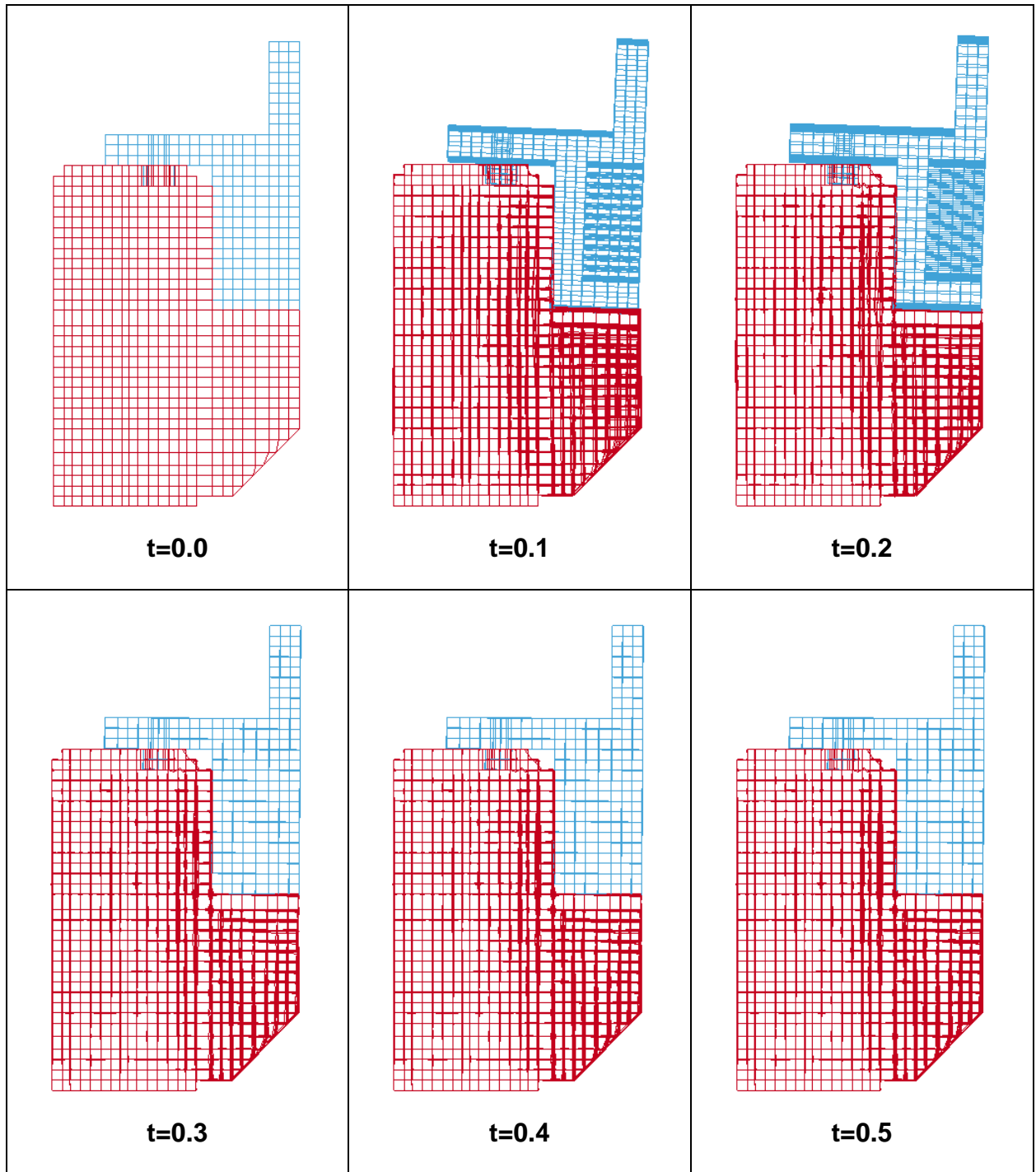Figure 38.   **Deformed Shapes: FEM-3. (t=0.0 to t=0.5)**

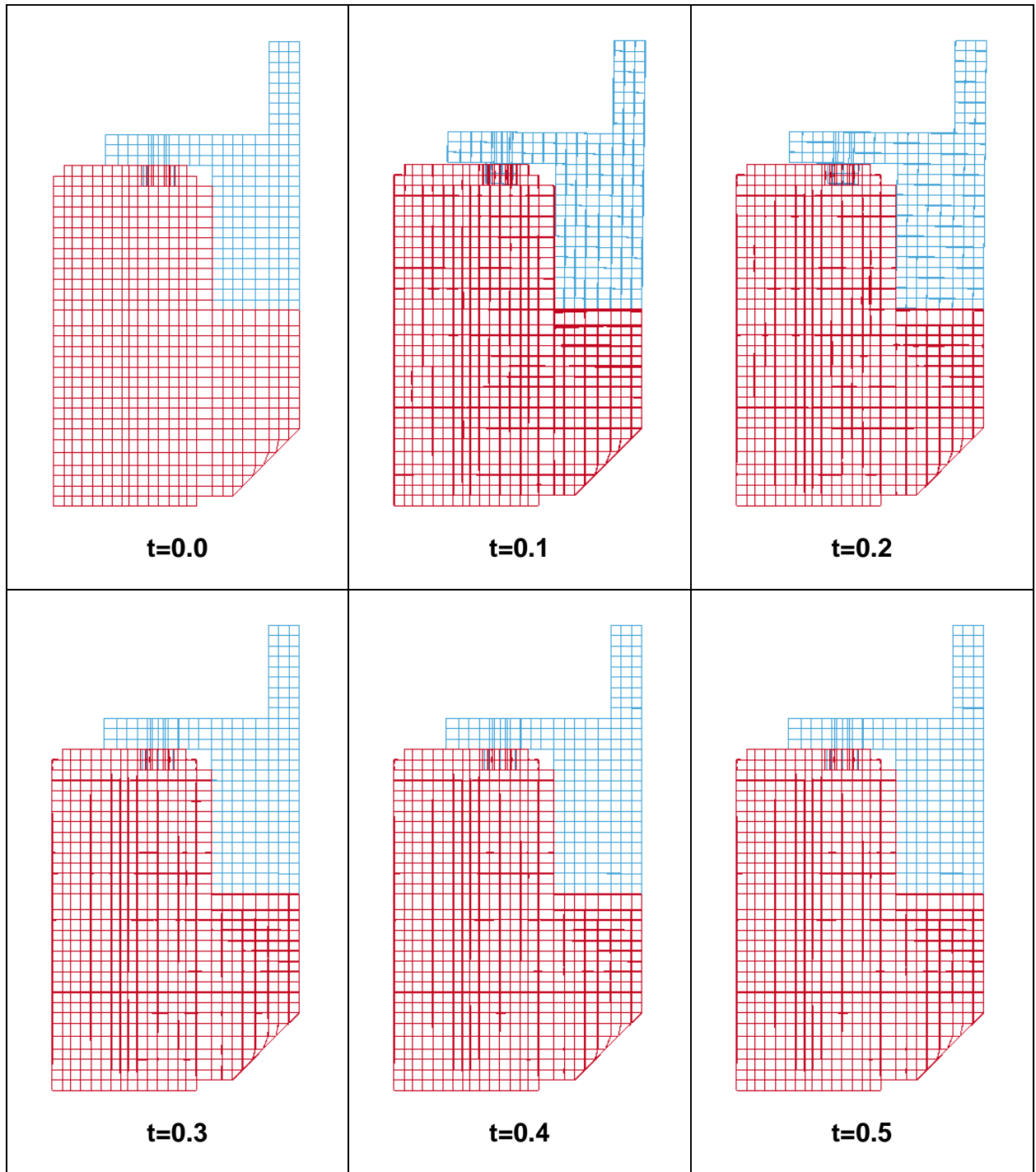Figure 39. **Deformed Shapes: FEM-4. (t=0.0 to t=0.5)**
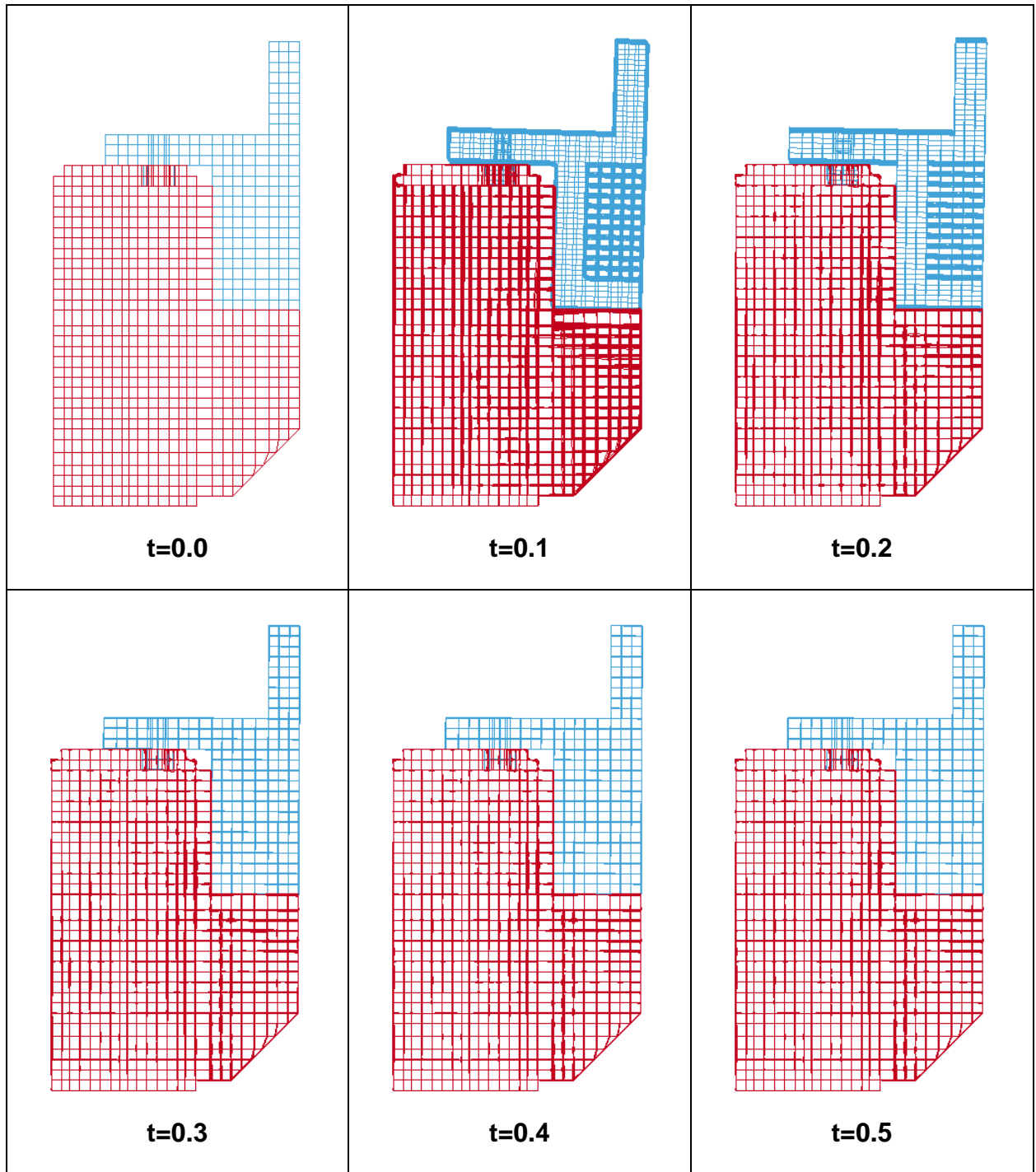
Figure 40.   **Deformed Shapes: FEM-5. (t=0.0 to t=0.5)**

43

Figure 41.   **Deformed Shapes: FEM-6. (t=0.0 to t=0.5)**
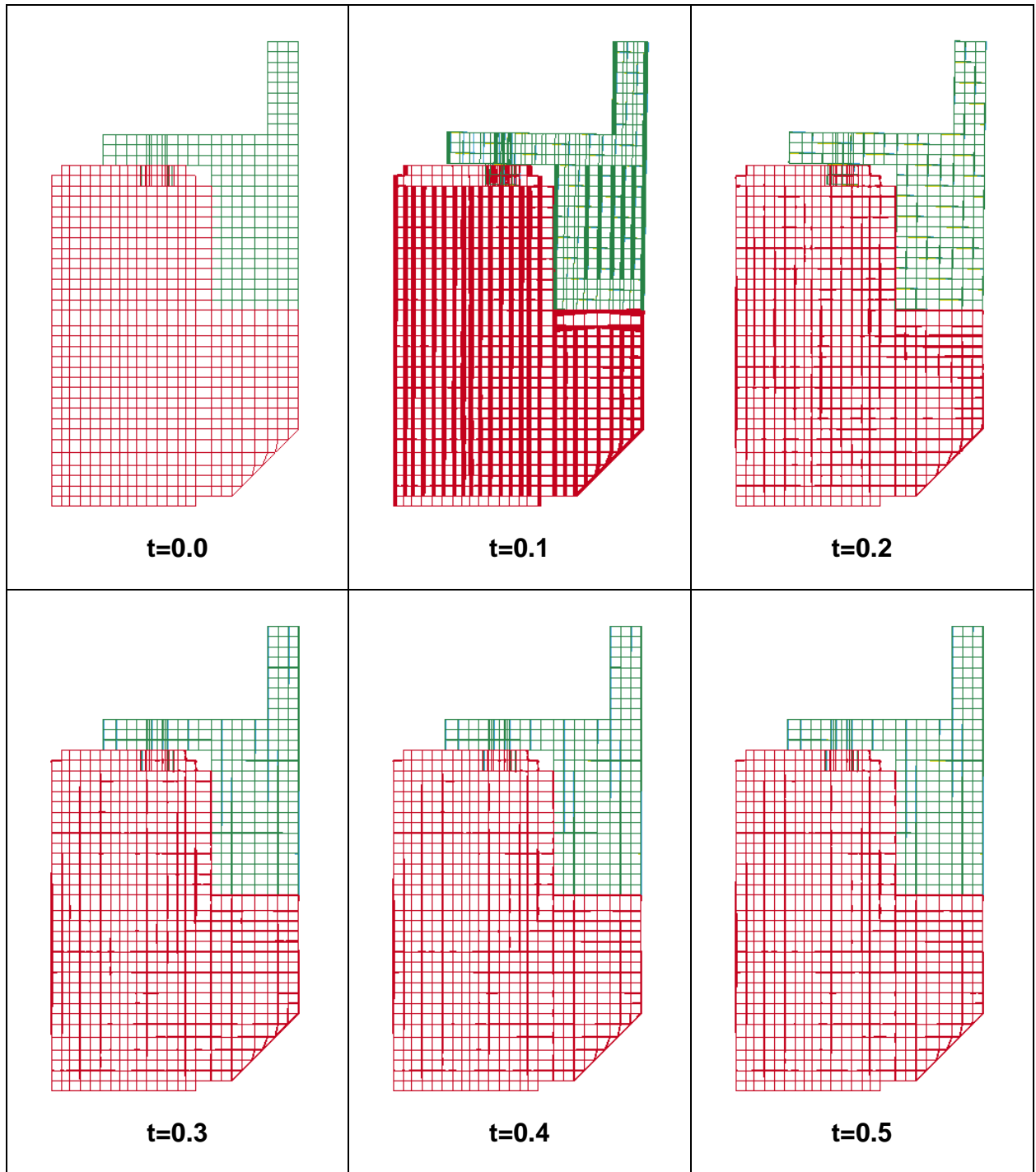
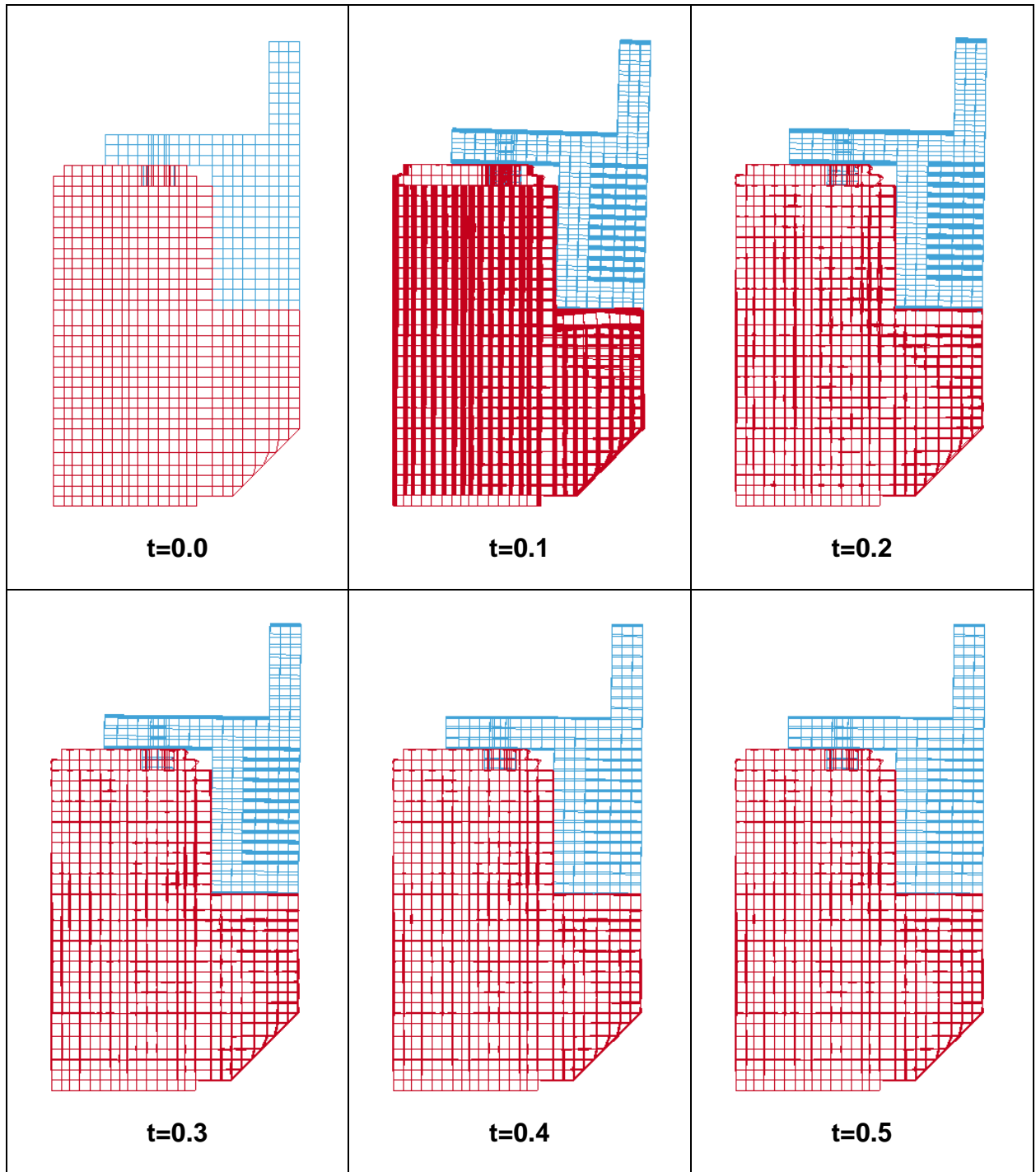Figure 42.   **Deformed Shapes: FEM-7. (t=0.0 to t=0.5)**

45

Figure 43. **Deformed Shapes: FEM-8. (t=0.0 to t=0.5)**

3.2.3 Discussion

3.2.3.1 Models FEM-1 to FEM-4

The following observations are made for models FEM-1 to FEM-4, which are all based on a 32-inch cross-beam spacing, by examining the stress plots and deformed shapes presented in Figure 28 to Figure 31 and Figure 36 to Figure 39, respectively:

1. The stresses resulting from side impact are substantially higher than those resulting from head-on impact. This is due to the fact that the impact load spreads across multiple guardrail modules in a head-on impact scenario;
2. The maximum von Mises stress in the beam resulting from head-on impact (FEM-1) is 32,710 psi concentrated around the shear pin holes. The maximum stresses in the beam otherwise are in the 10,000 to 13,000 psi range;
3. The maximum von Mises stress in the beam resulting from side impact occurs in FEM-2 and has a magnitude 80,150 psi. This stress is also concentrated around the shear pin holes, and the maximum stresses in the beam otherwise are in the 32,000 to 40,000 psi range;
4. The stresses obtained from side-impact models FEM-3 and FEM-4 are bounded by those obtained from model FEM-2;
5. The deformed shapes for all models (FEM-1 to FEM-4) demonstrate that the guardrail modules remain mounted after impact and do not become unlatched.

Based on these observations, the performance of the guardrails with the bolts removed is deemed acceptable. However, localized yielding can be expected to occur at shear pin holes.

3.2.3.2 Models FEM-5 and FEM-6

The following observations are made for models FEM-5 and FEM-6, which are both based on a 64-inch cross-beam spacing, by examining the stress plots and deformed shapes presented in Figure 32 to Figure 33 and Figure 40 to Figure 41Figure 39, respectively:

1. The maximum von Mises stress in the beam resulting from head-on impact (FEM-5) is 43,080 psi concentrated around the shear pin holes. The maximum stresses in the beam otherwise are in the 9,000 to 13,000 psi range;

2. The maximum von Mises stress in the beam resulting from side impact (FEM-6) is 80,260 psi concentrated around the shear pin holes. The maximum stresses in the beam otherwise are in the 32,000 to 40,000 psi range;

3. The deformed shapes for both models demonstrate that the guardrail modules remain mounted after impact and do not become unlatched.

Based on these observations, the performance of the guardrails with the bolts removed is deemed acceptable for a cross-beam spacing of 64 inches. However, localized yielding can be expected to occur at shear pin holes.

3.2.3.3 Models FEM-7 and FEM-8

The following observations are made for models FEM-5 and FEM-6, which are both based on a 64-inch cross-beam spacing, by examining the stress plots and deformed shapes presented in Figure 32 to Figure 33 and Figure 40 to Figure 41Figure 39, respectively:

1. The maximum von Mises stress in the beam resulting from head-on impact (FEM-5) is 54,740 psi concentrated around the shear pin holes. The maximum stresses in the beam otherwise are in the 27,000 to 33,000 psi range;

2. The maximum von Mises stress in the beam resulting from side impact (FEM-6) is 72,260 psi concentrated around the shear pin holes. The maximum stresses in the beam otherwise are in the 36,000 to 43,000 psi range;

3. The deformed shapes for both models demonstrate that the guardrail modules remain mounted after impact and do not become unlatched.

Based on these observations, the performance of the guardrails with the bolts removed is deemed acceptable for a cross-beam spacing of 96 inches. However, localized yielding can be expected to occur at shear pin holes.

4 CONCLUSIONS

In this study, eight unique finite element models were generated to simulate the impact scenarios outlined in Table 2 and evaluate the performance of the guardrail system when installed with the bolts removed.

A parametric study was carried out with three parameters evaluated, namely impact orientation, location of impact along the guardrail system, and cross-beam spacing used in the platform's top module. The first two parameters were selected to address the wide range of impact scenarios made possible by the RGVs' omni-directional travel capability, and the latter was selected in an attempt to optimize the platform design by reducing the number of cross-beams required.

The analysis was carried out in LS-DYNA, and evaluation of the guardrails' performance was achieved by comparing the output from LS-DYNA against the acceptance criteria established in Section 1.3.1.

The analysis results yielded the following conclusions:

1. the guardrail modules remain mounted and do not become unlatched upon impact when installed with the bolts removed;
2. the platform design can be optimized by reducing the number of cross-beams in the top modules and increasing the cross-beam spacing up to 96 inches;
3. the overall stresses in the platform sustained during impact are below the von Mises yield criterion, however localized yielding occurs at the shear pin holes. This is considered acceptable as the safety function of the guardrails is satisfied and no tear-out is experienced. However, it is recommended that hole locations be reinforced to keep the stresses in the platform within the elastic range.

REFERENCES

[R.1] Rolls-Royce Remote Tooling and Handling Systems. (n.d.). Retrieved December 16, 2017, from https://www.rolls-royce.com/~/media/ Files/R/Rolls-Royce/documents/customers/nuclear/ remotetoolinghandlingsystemstcm9259814.pdf

[R.2] Ontario Power Generation Performance Report for the Darlington Refurbishment Project. (n.d.). Retrieved December 16, 2017, from https://www.opg.com/darlington-refurbishment/Documents /DarlingtonRefurb_PerfomanceReport_July2014.pdf

[R.3] Wheelift Transporter Images and Videos. (n.d.). Retrieved April 03, 2018, from http://www.wheelift.com/resources-media/gallery#photo-gallery

[R.4] Atahan, A. O. (2002). Finite Element Simulation of a Strong-Post W-Beam Guardrail System. *Simulation, 78*(10), 587-599. doi:10.1177/0037549702078010001

[R.5] Hallquist, J. O. (2006). *LS-DYNA Theory Manual*.

[R.6] Hughes, T.J.R., Taylor R. L., Sackman, J. L., Curnier, A.C., and Kanoknukulchai, W. (1976). A Finite Element Method for a Class of Contact-Impact Problems. *J. Comp. Meths. Appl. Mechs. Eng. 8*, 249-276

[R.7] LS-DYNA Keyword User's Manual (Vol. I). (2016).

[R.8] Handbook of steel construction. (2016). CISC, Canadian Institute of Steel Construction.

[R.9] *S16-14 - Design of Steel Structures*. (2014). Toronto, Ont.: Canadian Standards Association.